VIETNAM NATIONAL UNIVERSITY, HANOI

**VIETNAM JAPAN UNIVERSITY**

**NGUYEN DANG QUANG HUY**

# STUDY OF MULTIPOLE EXCITATION OF PLASMON RESONANCE IN METAL NANOSTRUCTURE USING OPTICAL VORTICES

## MASTER'S THESIS

VIETNAM NATIONAL UNIVERSITY, HANOI

**VIETNAM JAPAN UNIVERSITY**

**_____**

**NGUYEN DANG QUANG HUY**

# STUDY OF MULTIPOLE EXCITATION OF PLASMON RESONANCE IN METAL NANOSTRUCTURE USING OPTICAL VORTICES

**MAJOR: NANOTECHNOLOGY**
**CODE: 8440140.11QTD**

**RESEARCH SUPERVISORS:**

**Dr. PHAM TIEN THANH**

**Hanoi, 2024**

# STATEMENT OF COMMITMENT

I am completely aware of the anti-plagiarism rules having studied them. I so promise with my honor that this research is my own and that it does not infringe the Regulation on Prevention of Plagiarism in Academic and Scientific Research Activities at Vietnam Japan University (issued jointly with Decision No 700/QD-DHBVN dated 30/09/2021 by the Rector of Vietnam Japan University). This thesis is submitted as part of the requirements for the master's degree in Nanotechnology. Any external sources utilized are duly acknowledged through explicit references.

**Signature**

**Nguyen Dang Quang Huy**

# ACKNOWLEDGMENTS

This thesis will be a mark for me to keep developing myself and keep going on the scientific path. Hence, I am deeply grateful to my advisor, Doctor Pham Tien Thanh, who guided me throughout the dissertation process. Moreover, I appreciate Prof Tanaka Daisuke for guiding me in running the simulation and Prof Nguyen Viet Hung for helping me research this thesis's basic theory.

I sincerely thank all my family and friends, who have always supported me and helped me with my difficulties throughout the process. All your support is my motivation to complete my thesis.

Lastly, I am grateful to the VietNam Japan University for providing the resources and facilities necessary to complete this thesis.

Nguyen Dang Quang Huy

HaNoi, July 17, 2024

Table Of Contents

ABSTRACT.....v
CHAPTER 1: METAL NANOSTRUCTURE AND PLASMON EFFECT .....1
1.1 Metal nanostructure .....1
*1.1.1 History and present application of metal nanostructure* .....1
*1.1.2 Application of metal nanostructure* .....1
1.2 Surface plasmon resonance effect - SPR.....3
*1.2.1. Introduction*.....3
*1.2.2. Model of surface plasmon effect on metal nanoparticles* .....3
*1.1.1 Multipole plasmon resonance* .....4
CHAPTER 2: OPTICAL VORTEX .....6
2.1 Introduction to Optical Vortex.....6
2.2 Classical model of optical vortex.....7
*2.2.1 Laguerre-Gaussian mode (LG)* .....7
*2.2.2 Hermite-Gaussian mode (HG)* .....8
2.3 Creation of optical vortex .....8
*2.3.1 Spiral phase plate*.....8
*2.3.2 Spatial light modulator*.....10
2.4 Application of Optical Vortex .....10
*2.4.1 Optical tweezers* .....10
*2.4.2 Optical comunication* .....11
CHAPTER 3: RESULTS AND DISCUSSION .....12
3.1 Simulation model.....12
3.2 Gold nano plate.....13
*3.2.1 Circular gold nano plate* .....13
3.3 Square gold nanoplate.....16
3.4 Metal-insulator-metal structure (MIM).....19
*3.4.1 First structure: Gold plate - Insulator ring - gold ring*.....20
*3.4.2 Second structure: empty gold plate - PMMA ring - gold ring* .....22
*3.4.3 Third structure: Sandwich structure* .....24
CHAPTER 4: RESULTS AND CONCLUSIONS .....27
APPENDIX B. GENERATE CIRCULAR DISK C CODE .....31
APPENDIX C. ROUGH ESTIMATION OF SPR.....32
APPENDIX D. DISCRETE DIPOLE SCATTERING PROGRAM .....34
REFERENCES .....36

# LIST OF FIGURES

**Figure 1.1.** Lycurgus cup with different colors. It shows blue jade when illuminated from the outside. It shows red when illuminated from the inside. [5] .....1
**Figure 1.2.** Schematic illustration of the mechanism of SERS for detection of analytes [9].....2
**Figure 1.3.** Schematic illustrates a model for plasmon oscillation. [10].....4
**Figure 1.4.** Schematic illustrates multipole surface plasmon resonance state. (a)Dipole state. (b)Quadrupole state. (c)Hexapole state.....5
**Figure 2.1.** Roadmap of the 30-year development of optical vortices from 1989 to 2019, including significant theoretical and technical breakthroughs with corresponding references. [13].....6
**Figure 2.2.** The profile of LG3 beam mode from left to right is the side view of the electric field, the top view of the electric field, and the phase of the electric. The figure in each line corresponds to p equal to 0,1,2 respectively .....7
**Figure 2.3.** Profile of Hermite Gaussian mode with different n and m. From the first line to the last line represents for n = 0 to 2 respectively and from left to right represents for m = 0 to 2.....9
**Figure 2.4.** Design of the spiral phase plate to create an optical vortex from a Gaussian beam. The red plane is present for the phase of the beam. [14].....9
**Figure 2.5.** Schematic of SLM structure and SLM in real optical system. [21] [22]...10
**Figure 2.6.**1µm diameter beads circulate when held in an optical vortex. [15].....10
**Figure 2.7.** Schematic illustration for using optical vortex for communication underwater. [17].....11
**Figure 3.1.** The simulation schematic.....13
**Figure 3.2.** Scattering and absorption spectrum of gold nanoplate. .....13
**Figure 3.3.** The near field distribution of gold nanoplate in four cases. .....15
**Figure 3.4.** Absorption and Scattering spectrum of gold nanoplate with R = 80, 100, 120 nm and d = 10 nm. .....16
**Figure 3.5.** Absorption and Scattering spectrum of gold nanoplate with d = 10, 20, 30 nm and R = 10 nm .....16
**Figure 3.6.** Absorption and scattering spectrum of gold square nanoplate .....17
**Figure 3.7.** Near field electric distribution of gold square nanoplate.....18
**Figure 3.8.** Schematic of MIM model structure. The left picture is the visualization model of the MIM structure. The right picture is the structure after discretized. .....19
**Figure 3.9.** Absorption and scattering spectrum of MIM (a),(b) and the outside ring only (c)(d). The middle layer in this case is the vacuum. .....21
**Figure 3.10.** Electric field distribution of MIM structure at absorption peak. .....22
**Figure 3.11.** Absorption and scattering spectrum of the first model with vacuum and PMMA layer at different r. The dashed line shows the result with PMMA and the

filled line shows the vacuum result. .....22
**Figure 3.12.** Absorption and scattering spectrum of the second model depend on the hole's radius.....23
**Figure 3.13.** Electric distribution with different hole radii. The left figure to the right shows electric distribution with $r_2$ equal to 30 nm and 50 nm respectively. .....23
**Figure 3.14.**The sandwich model's Absorption and Scatxtering spectrum depend on the PMMA layer's thickness excited by the LG beam. .....24
**Figure 3.15.** The linear dependence between resonance wavelength and the PMMA thickness. .....25
**Figure 3.16.** Crossection electric field distribution. (a) Along the sample. (b) On the gold surface. (c) On the PMMA layer. .....26

# LIST OF TABLES

**Table 3.1.** The selective rule of multipole plasmonic formation.....14
**Table 3.2.** Table shows the resonance wavelength with different PMMA thicknesses.....25

## ABBREVIATIONS

**HG:** Hermite-Gaussuan mode.
**LCP:** Left Circular Polarization.
**LG:** Laguerre-Gaussian mode.
**LSPR:** Localized Surface Plasmon Resonance.
**MIM:** Metal-Insulator-Metal structure.,
**MPR:** Multipole Plasmon Resonance.
**OAM:** Orbital Angular Momentum.
**OVs:** Optical Vortices.
**PMMA:** Poly methyl methacrylate.
**RCP:** Right Circular Polarization.
**SAM:** Spin Angular Momentum.
**SERS:** Surface Enhanced Raman Scattering.,
**SPR:** Surface Plasmon Resonance.,
**TAM:** Total Angular Momentum.

# ABSTRACT

Since 19$^{th}$ century, nanomaterial has been considered a promising material that can create a big jump in technology due to its special properties. The reason for the difference is based on the size effect of the material. With nanoscale size, the number of surface atoms increases significantly and takes a pivotal role in forming the material properties. Hence, the surface plasmon resonance effect becomes sig- nificantly strong in the nanomaterial. The plasmon effect was observed in the early 20$^{th}$ century by Prof Robert W. Wood and under research the following time. Up to now, Surface Plasmon Resonance (SPR) has been applied in many fields such as bio-detection, solar cells, and surface-enhanced Raman scattering. However, in the late 20$^{th}$ century Optical Vortices (OVs) was discovered as a new type of light with a topological charge and singularity in the optical axis. This light creates a new plasmon effect known as the Multipole Plasmon Resonance (MPR). In this thesis, I investigate the formation of the multipole plasmon resonance effect on metal nanostructures with different shapes and sizes. I use the DDSCAT program to simulate the interaction of a Laguerre-Gaussian beam (one mode of optical vor- tex) with the sample. Then, by analyzing the absorption and scattering spectrum we come up with the dependence of the MPR wavelength on the shape and size of the sample. By looking at the near-field electric distribution of the sample we can conclude the connection between the MPR state with the topological charge. Overall, my thesis provides a basic phenomenon about the MPR effect which is created by a Laguerre-Gaussian beam. This result can be used as reference in- formation for future research in optical manipulation, optical communication, and optical properties of material.



**Keywords:** metal nanostructure, DDSCAT, Lagurre-Gaussian beam, Optical vor tex, multipole plasmon resonance


**Research purpose:**

Investigate the formation of plasmon multipole states caused by the optical vortex.

**Research method:**

Approaching the creation of plasmon multipole states due to the optical vortex experimentally is very difficult. So, in this thesis, I use the open-source code DDSCAT to simulate the interaction of OVs with the metal nanostructure. My thesis consists of four parts:

- Chapter 1: Metal nanostructure and plasmon effect.
- Chapter 2: Optical vortex
- Chapter 3: Result and conclusion
- Chapter 4: Conclusion

# CHAPTER 1: METAL NANOSTRUCTURE AND PLASMON EFFECT

## 1.1 Metal nanostructure

### *1.1.1 History and present application of metal nanostructure*

**Figure 1.1.** Lycurgus cup with different colors. It shows blue jade when illuminated from the outside. It shows red when illuminated from the inside. [5]

In ancient times, metal nanostructures such as gold and silver particles were accidentally synthesized without a deep understanding. These materials were used to make coins and jewelry at that time. Later in the Middle Ages gold nanoparticles were used for color glasses. The most famous colored glass work at that time was the Lycurgus cup which can change its colors when illuminated from outside and inside [5, 7]. In the late 20th century, the metal nanostructure was investigated for the first time with the development of electron microscopy and X-ray diffraction techniques. Since then, many metal nanostructure properties have been researched and applied in many practical applications. The most common application can be considered as the photocatalyst and surface-enhanced Scattering (SERS). In the future, metal nanostructures are promising to be applied in drug delivery, quantum computing, etc.

### *1.1.2 Application of metal nanostructure*

**a.Photocatalyst**

Now, people have to deal with many problems such as environmental pollution

and the production of organic material. These problems require a novel catalyst to enhance the speed of chemical reactions with light. Metal nanomaterials are a suitable solution for this issue. Firstly, the metal nanostructure can absorb the broad spectrum of light even UV light which is needed for the catalyst due to the plasmon effect. Moreover, by changing the size, shape, and material scientists can tune the SPR wavelength to be suitable for the incident light. Now, many metal nanostructures have been used for photocatalysts such as silver nanoparticles, gold nanoparticles, and platinum nanoparticles. Silver and gold nanoparticles are used to degrade organic pollutants in water [6] [7]. Platinum nanoparticles with the ability to absorb UV light have been employed as photocatalyst material in water-splitting reactions for hydrogen production [8].

### b.Surface Enhanced Raman Scattering – SERS

Surface-enhanced Raman Scattering is a powerful technique to detect molecules on the sample by detecting Raman scattering beams. In this method, scientists coat a thin metal layer, such as silver or gold, on the substrate. Then when the incident laser interacts with the sample to create the Raman backscattering beam it also interacts with the thin metal layer below. This layer makes the electric field to enhance the Raman signal due to the Localized Surface Plasmon Resonance (LSPR) effect. Figure 1.2 illustrates the working principle of the SERS.

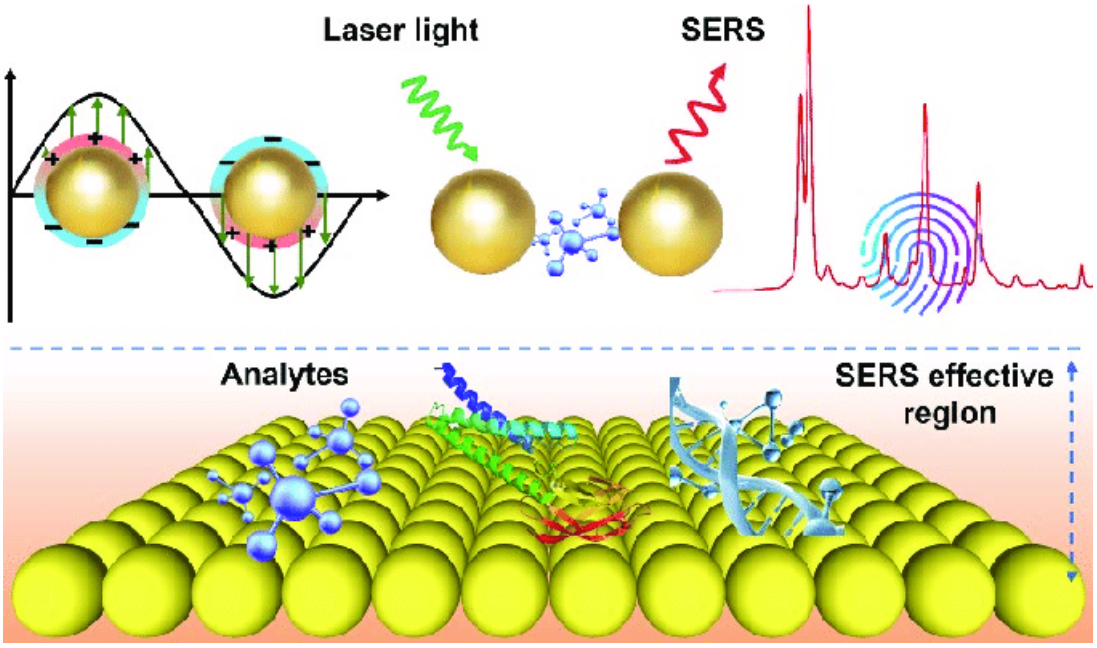


**Figure 1.2.** Schematic illustration of the mechanism of SERS for detection of analytes [9]

## 1.2 Surface plasmon resonance effect - SPR

### *1.2.1. Introduction*

Surface plasmon resonance is a physical phenomenon between the plasma oscillations of the electron with an incident light with a specific frequency. This effect depends on the size, shape, material, and index of ambient material. At the resonance frequency, the electric field around the material is greatly enhanced which leads to the strong interaction of the material with light. In some way, meta nanostructure can be considered as a resonance generator of surface plasmon resonance. Applications of metal nanostructures are based on different behaviors of the SPR effect. Biological sensing and optical filters use extinction and absorption properties which are based on the SPR effect. Waveguide applications are based on the nearfield interaction at the resonance wavelength. Surface-enhanced Ra- man scattering and Surface-enhanced fluorescence are based on both near-field and far-field interaction of resonantly excited metal nanoparticles. Overall, most applications of metal nanostructure come from the SPR effect.

### *1.2.2. Model of surface plasmon effect on metal nanoparticles*

To understand the SPR effect clearly, we consider the interaction of light with metal nanoparticles that have a size smaller than the penetration depth of incident light ($\sim$ 20 nm for silver and $\sim$ 26 nm for gold) [10]. The electric field of the light makes the free electron shift from its lattice. This state of the system can be considered as a dipole. The Coulomb force of the ion lattice pulses back the free electron cloud to the normal state while the light keeps pulling and pushing the electron. These forces make the free electron cloud do a forced oscillation. Therefore, with a suitable frequency, the oscillation gets resonance and absorbs most of the energy from the incident light. This phenomenon is called surface plasmon resonance (SPR). With this model, we can explain why metal materials often have higher absorption rates at the ultra-violet region and give rough estimates of the resonance wavelength. The estimation is shown in Appendix C

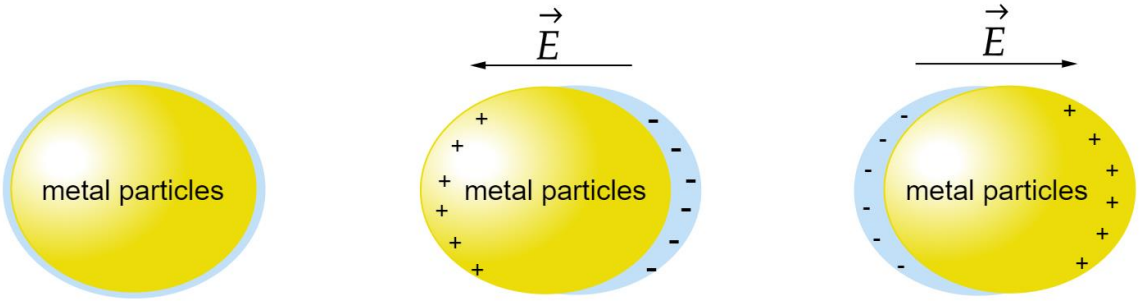


**Figure 1.3.** Schematic illustrates a model for plasmon oscillation. [10]

Most of the SPR effect can be understood by the above model. However, we can split the SPR effect into two main types local surface plasmon resonance (LSPR) and surface plasmon resonance (SPR). The LSPR occurs in small metal nanoparticles much smaller than the wavelength of the incident light. This effect creates an electric field in the near field of the nanoparticles. Hence, in SERS we coat a layer of the nanoparticles in the substrate. This layer will create an extra electric field that enhances the Ramman scattering signal. SPR occurs in 2D material such as thin film. SPR can propagate for a long distance in the surface of the thin film which can reach to micrometers. So, this effect is often used in image and plasmon sensing.

### *1.2.3. Multipole plasmon resonance*

Multipole plasmon resonance is the excited state of the SPR effect. Normally, with the linear polarization beam and asymmetric structure, we can easily observe the dipole state of the metal nanostructure. By adjusting the sample structure to have many sharp points we can create the multipole state due to the LSPR effect. The second method is adding a new part to the structure. This part will make the coupling effect and more poles in the structure. The last method is changing the incident light to the structure light such as azimuthally beam and optical vortex. The first two methods have been investigated in detail in many articles [11] [12]. Hence, in this thesis, I try to examine the formation of multipole plasmon resonance by using the optical vortex.

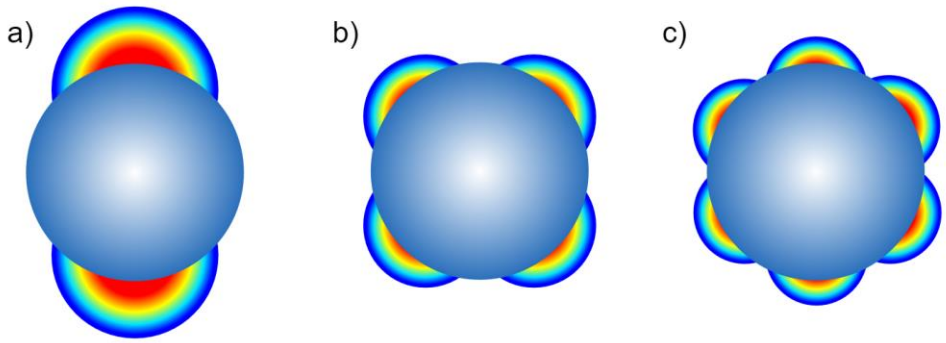


**Figure 1.4.** Schematic illustrates multipole surface plasmon resonance state. (a)Dipole state. (b)Quadrupole state. (c)Hexapole state.

# CHAPTER 2: OPTICAL VORTEX

## 2.1. Introduction to Optical Vortex

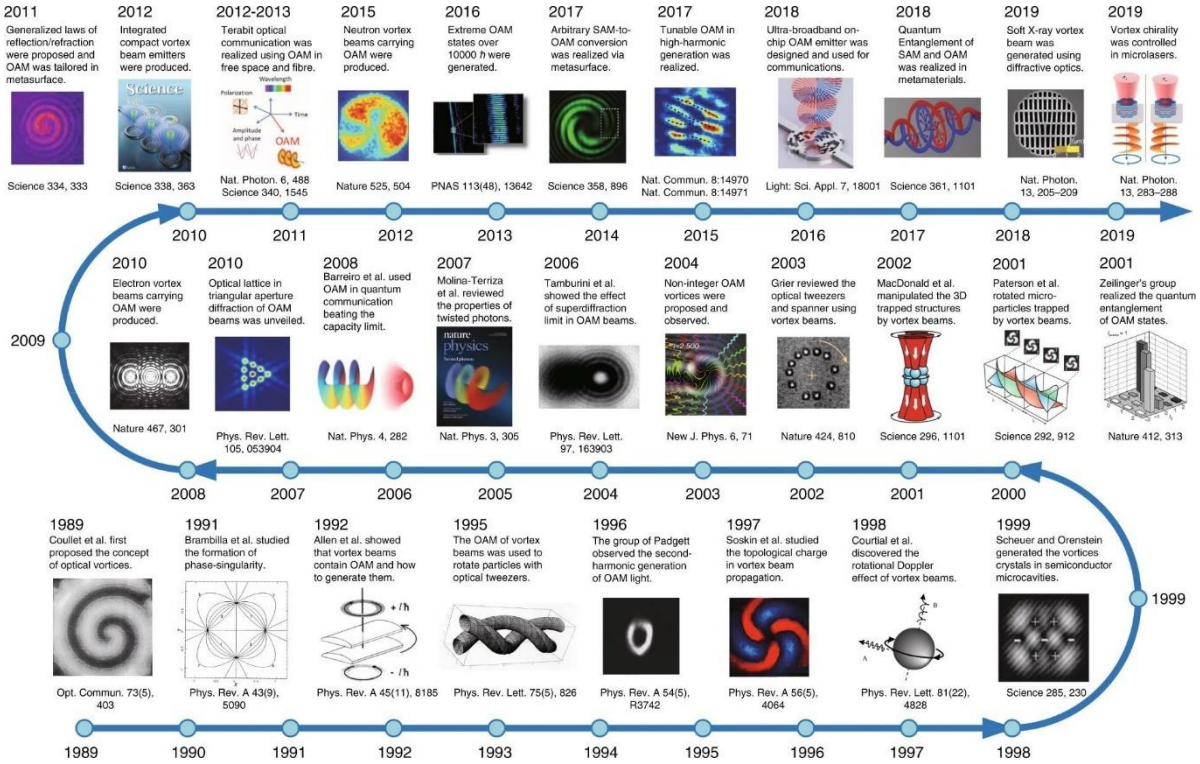


**Figure 2.1.** Roadmap of the 30-year development of optical vortices from 1989 to 2019, including significant theoretical and technical breakthroughs with corresponding references. [13]

Optical Vortices (OVs), also known as vortex beam or vortex light, have been a popular topic for the last 30 years. The optical vortex's unique structure appeals to many scientists. With a phase singularity in the optical axis, the optical vortex forms a black patch in the middle of the beam and a donut-shaped waveform. In 1989, Coulleet et al introduced the optical vortex concept by solving the Maxwell equation in cylinder coordinates. Three years later, Allen's work demonstrated the orbital angular momentum of Vortex beams, revealing a novel link between macroscopic optics and quantum effects. In the theoretical field, the OVs are characterized by the term $e^{i\ell\theta}$, equal to $\ell\hbar$ Orbital Angular Momentum (OAM) which is much higher than the Spin Angular Momentum (SAM) of the beam. The SAM of the Vortex beams is related to the polarization of the beam which has two values $\pm\hbar$ standing for Left Circular Polarization (LCP) and Right Circular Polarization (RCP) respectively. Since then, a lot of research has been conducted to build fundamental theories and investigate the

properties and application of optical vortexes [13].

## 2.1. Classical model of optical vortex

### *2.1. Laguerre-Gaussian mode (LG)*

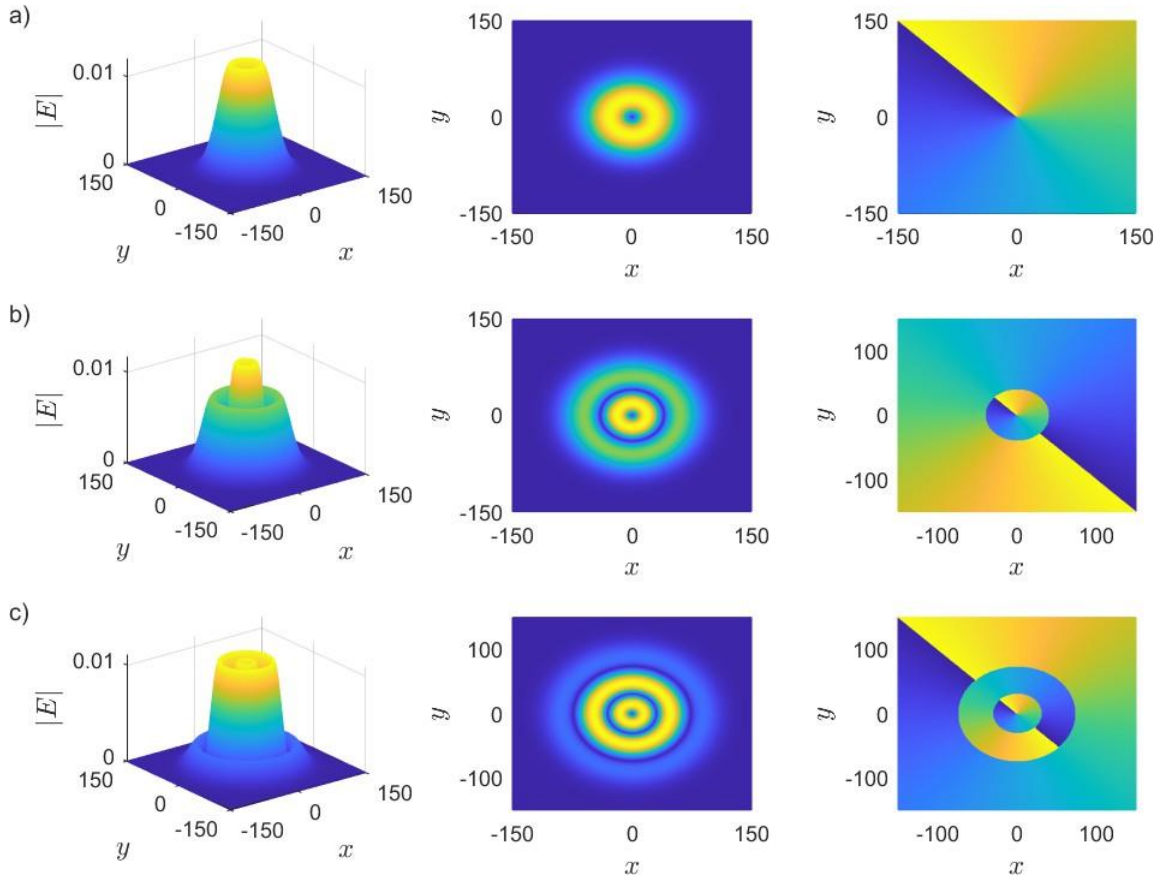


**Figure 2.2.** The profile of LG3 beam mode from left to right is the side view of the electric field, the top view of the electric field, and the phase of the electric. The figure in each line corresponds to p equal to 0,1,2 respectively

The most popular mode of Vortex beam is the LG mode. This mode has axial symmetry and can be easily created by a spiral phase plate. The equation for the LG mode is given as:

$$LG_p^l(r,\phi,z) = \sqrt{\frac{2p!}{\pi(p+|l|)!}}\left(\frac{\sqrt{2}r}{\omega(z)}\right)^l L_p^{|l|}\left[\frac{2r^2}{\omega(z)^2}\right] \frac{\omega_0}{\omega(z)}\exp\left(-\frac{r^2}{\omega(z)^2}\right)\exp(il\phi) \exp\left[-i\left(1+2p+|l|\tan^{-1}\left(\frac{z}{z_R}\right)\right)\right] \exp\left(-i\frac{kr^2}{2R(z)}\right)\exp(ikd) \quad (1)$$

where $\omega$ is the beam diameter, $L_p$ is the Laguerre polynomial, and $R(z)$ is the radius of the curvature. $\ell$ represents the orbital angular momentum and $p$ describes the number of the ring (radial part), $k$ is the wave number. With $\ell = 0$ and $p = 0$, the LG mode will become a normal Gaussian beam.

### *2.2. Hermite-Gaussian mode (HG)*

Like the LG mode Hermite-Gaussuan mode (HG mode) also has axial symmetry and can be created through the hologram or spiral phase plate. However, unlike LG mode the phase of the HG mode separates into different constant phase domains. The special property of HG mode and LG mode is that they are orthogonal to each other, hence we can decompose the LG mode into the linear combination of HG mode and reverse. This property raised the idea of using it for optical communication. Because of that, the discovery of a new form of optical vortex has led to several new applications. The equation for HG mode is displayed as:

$$E_{nm}(x,y,z) = E_0 \frac{\omega_0}{\omega(z)} H_n\left(\sqrt{2}\frac{x}{\omega(z)}\right) \exp\left(-\frac{x^2}{\omega(z)^2}\right)$$
$$H_n\left(\sqrt{2}\frac{y}{\omega(z)}\right) \exp\left(-\frac{y^2}{\omega(z)^2}\right)$$
$$\exp\left(-i\left[kz - (1+n+m)\,tan^{-1}\frac{z}{z_R}\right]\right)$$
$$\exp\left(-i\frac{k(x^2+y^2)}{2R(z)}\right)$$

$H_n(x)$ is the Hermitian polynomial function. Numbers $n$ and $m$ determined the shape of the HG mode in $x$ and $y$ direction.

## 2.3. Creation of optical vortex

### *2.3.1. Spiral phase plate*

The main principle to create the optical vortex is by letting constant phase plane waves go through the transparent environment to create a variety of phases. The most common method for this rule is using the spiral phase plate called a vortex lens. The vortex lens is a plate whose refractive index depends

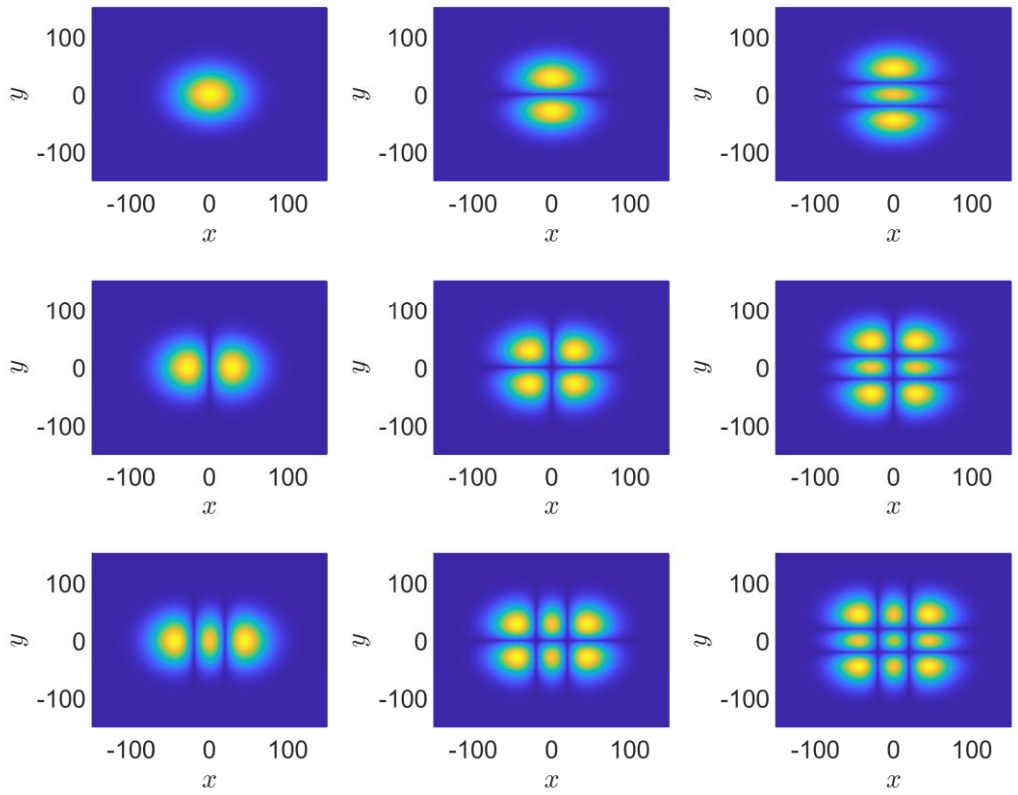


**Figure 2.3.** Profile of Hermite Gaussian mode with different n and m. From the first line to the last line represents for n = 0 to 2 respectively and from left to right represents for m = 0 to 2.

on the angle. To create this property we can adjust the plate's thickness or refractive index. Figure 2.4 shows the main working principle of the spiral phase plate. Due to the complexity and precision of the structure, 3D printing and photolithography are the most reliable methods to construct these lenses.

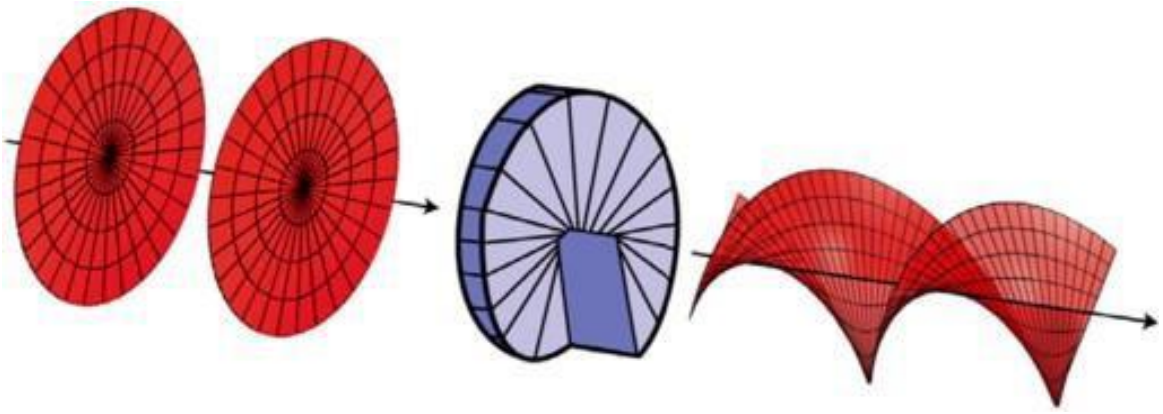

**Figure 2.4.** Design of the spiral phase plate to create an optical vortex from a Gaussian beam. The red plane is present for the phase of the beam. [14]

### *2.3.2. Spatial light modulator*

The spatial light modulator is one of the most flexible methods to create an optical vortex. Similar to the spiral phase plate the main rule of the spatial light modulator is to create a graded index that depends on the angle to vary the phase of the income light. The basic spatial light modulator system consists of four layers: the electrode, liquid crystal, alignment, and glass substrate. By applying a voltage between the electrode layer the spatial light modulator system can change the orientation of the liquid crystal layer and then vary this layer's refractive index at each point. This property allows the spatial light modulator system to create phase patterns easily.

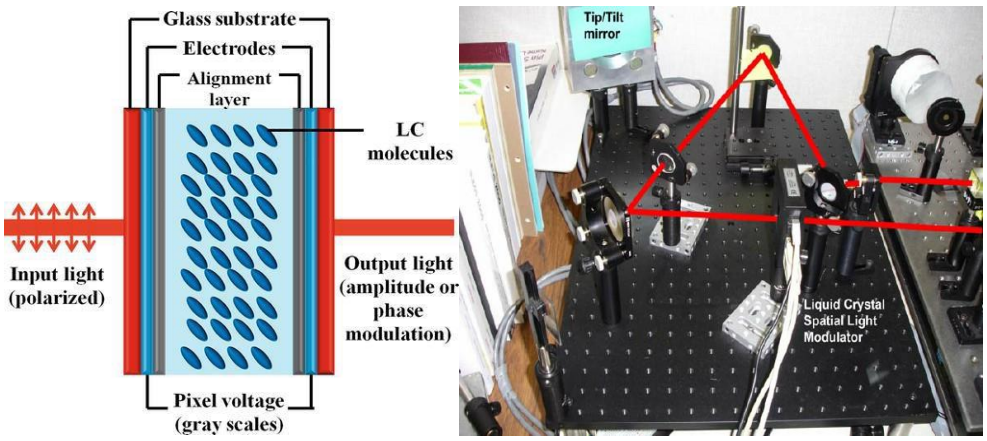


**Figure 2.5.** Schematic of SLM structure and SLM in real optical system. [21] [22]

## 2.4. Application of Optical Vortex

### *2.4.1.Optical tweezers*

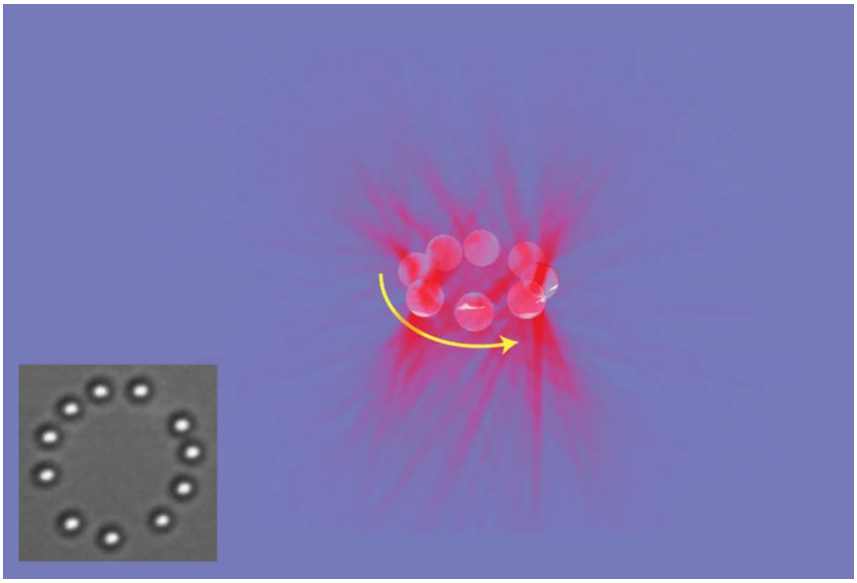

**Figure 2.6.**1μm diameter beads circulate when held in an optical vortex. [15]

Askin who won the Nobel prize in 2018, proposed the optical tweezers in 1970 using optical force to control the particles. Based on that idea, OVs were applied in this field in 1995 for the first time. OVs with OAM and SAM allow scientists to control the position, rotation, and spin of the particle at the same time [15]. Hence, the guiding ability of the optical tweezers becomes more flexible. This guiding ability of optical tweezers can be applied to drug delivery and targeted therapy in biomedical. Moreover, OVs can trap dielectric particles in the singularity point through the plasmon effect [16]. Hence, it can be applied in nanotechnology and nano-manipulation.

### *2.4.2. Optical comunication*

The most popular application of optical vortex is in optical communication. Normally, the information is encoded through the polarization, frequency, and pulse shape. Now, with optical vortex the orbital angular momentum can be considered as a new degree of freedom for multiplexing modulation. This application has enlarged the capacity of optical communication and broken the Tbit level. Moreover, with the development of a femtosecond vortex beam, communication speed was enhanced. OAM multiplexing-based communication was also demonstrated under many extreme circumstances, such as underwater communication, high-dimensional quantum communication, and long-distance fiber communication [17] [18].

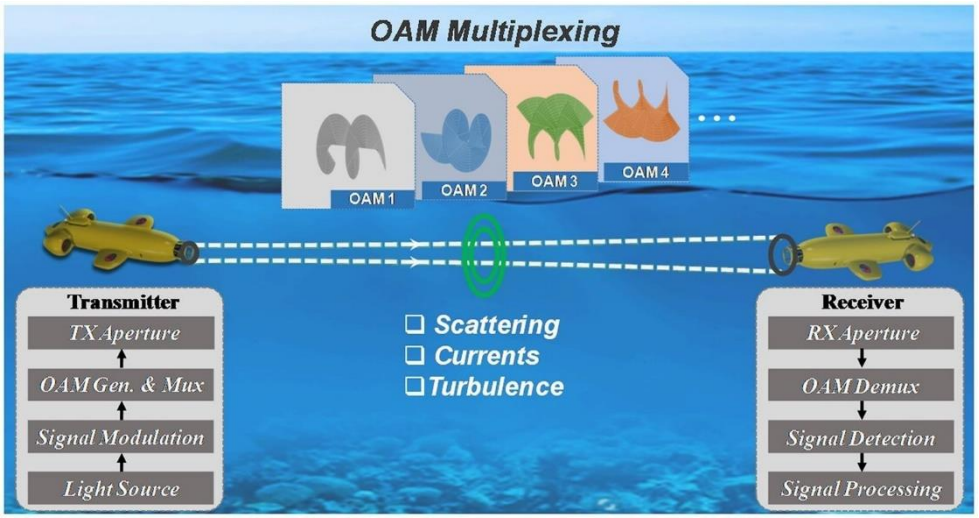


**Figure 2.7.** Schematic illustration for using optical vortex for communication underwater. [17]

# CHAPTER 3: RESULTS AND DISCUSSION

## 3.1. Simulation model

The extinction, absorption, scattering, and nearfield electric distribution are used to consider the dependence of the plasmonic effect on the angular momentum. The incident beam is the Laguerre-Gaussian beam with different OAM ($\ell$) and the SAM ($s$) is set to ±1. To simplify, The LG beam is set to be the single-ring beam ($p$ = 0). For convenience, we denote the LG beam with TAM $\ell$ and SAM $s$ as $LG_{\ell s}$. The beam is exposed perpendicular to the sample's surface. Because the sample thickness in this simulation is minimal compared to the wavelength, we can assume that the beam waist is constant along the propagation direction So we have $\omega = \omega_0$, Rayleigh length, and radius curvature become $\infty$ ($R(z) = z_R = \infty$). Hence the equation represents the source becomes:

$$E_x = E_0 \left(\frac{\sqrt{2}r}{\omega_0}\right)^{|l|} \exp\left(-\frac{r^2}{\omega_0^2}\right) \exp(\mathrm{i}l\phi) \tag{2}$$

$$E_y = \mathrm{i}sE_0 \left(\frac{\sqrt{2}r}{\omega_0}\right)^{|l|} \exp\left(-\frac{r^2}{\omega_0^2}\right) \exp(\mathrm{i}l\phi) \tag{3}$$

$$E_z = 0 \tag{4}$$

The number $s$ shows the polarization state of the incident light corresponding to two values ±1 for two states left circular polarization and right circular polarization. The beam waist ($\omega_0$) is set to focus on the sample hence it is smaller than the radius of the sample. The structures we investigate are the nanoplate with different shapes and sizes. All structures are made from gold. The refractive index of gold is taken from Johnson and Christy's results [19]. Nanostructures that have sizes smaller than 200 nm × 200 nm show a stronger SPR effect, therefore, we expect the size parameter around 150 nm and the thickness around 10 nm approx half of the mean penetration depth of normal light. The schematic of the simulation model is shown in Figure 3.1.

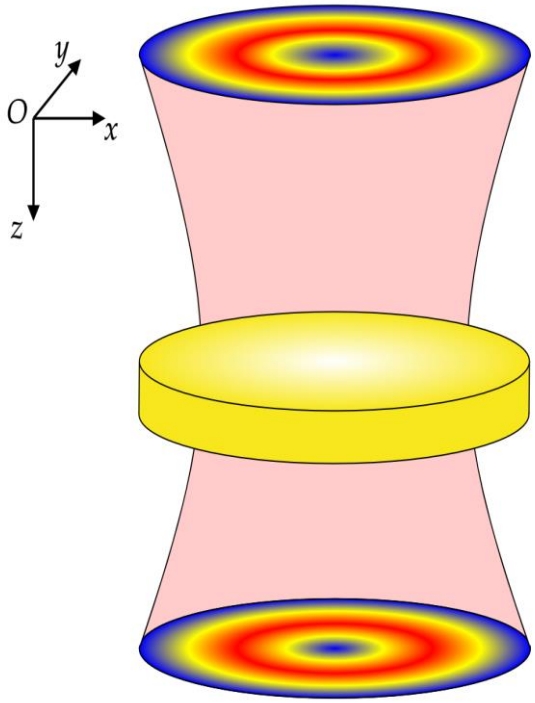


**Figure 3.1.** The simulation schematic.

## 3.2 Gold nano plate

### *3.2.1 Circular gold nano plate*

### a. The dependence of MPR on OAM and TAM

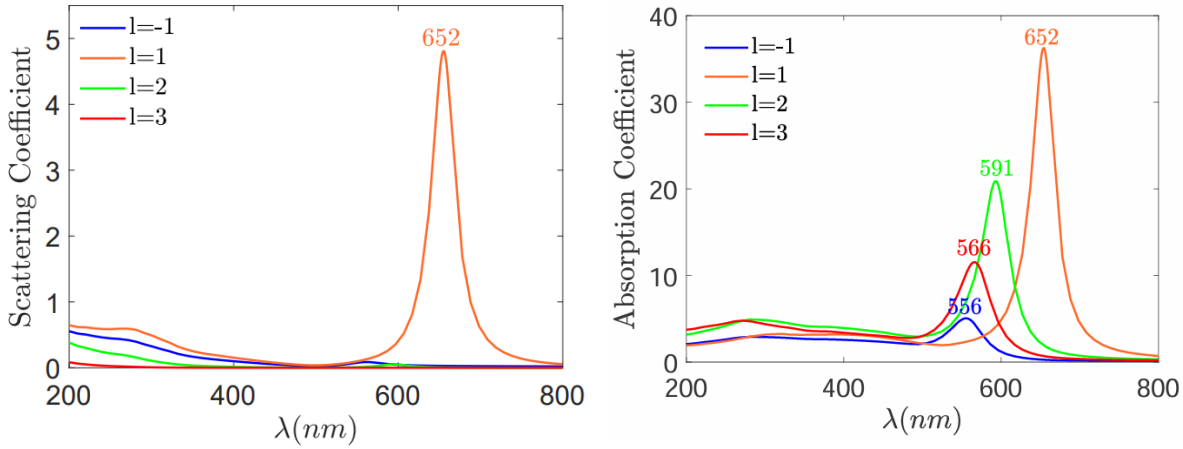


**Figure 3.2.** Scattering and absorption spectrum of gold nanoplate.

Figure 3.2 shows the absorption and scattering spectrum of gold nanoplate whose radius is 100 nm and its thickness is 10 nm. The incident beam used in this simulation is $LG_{\ell 1}$ with $\ell$ changing from $-1$ to 3. The scattering and absorption properties of gold nanoplate depend on the orbital angular momentum. The sample shows the highest scattering properties with the mode $LG_{11}$ at 652 nm. Meanwhile, the absorption spectrum shows peaks at 556 nm, 657 nm, 596 nm, and 566 nm with

$\ell$=−1, 1, 2, 3 respectively. The absorption spectrum indicated that the light that has total angular momentum shows a better absorption rate. However, when increasing the orbital angular momentum the absorption peak decreases and shifts to a higher frequency. It is assumed that this effect is due to the formation of the multipole plasmonic.

**Table 3.1.** The selective rule of multipole plasmonic formation

| Plasmonic mode | TAM | SAM | OAM |
|---|---|---|---|
| No State | 0 | 1<br>-1 | -1<br>1 |
| Dipole | 1 | 1<br>-1 | 0<br>2 |
| | -1 | -1<br>1 | 0<br>-2 |
| Quadrupole | 2 | 1<br>-1 | 1<br>3 |
| | -2 | 1<br>-1 | -3<br>-1 |
| Hexapole | 3 | 1<br>-1 | 2<br>4 |
| | -3 | -1<br>1 | -2<br>-4 |

Figure 3.3 shows the electric field distribution around the circular gold nanoplate at the absorption peaks in each case. Without the total angular momentum, the plasmonic effect can not be created on the sample. However, the multipole plasmon resonance is observed in the other cases. This result also indicated a linking rule between the number of plasmonic poles and the total angular momentum: the number of poles is double the TAM number. Hence, the selective state of multi-pole plasmonic can be created through the suitable combination of orbital angular and spin angular momentum. Some combinations have been listed in Table 3.1. This result shows the same result as the reference result in [20].

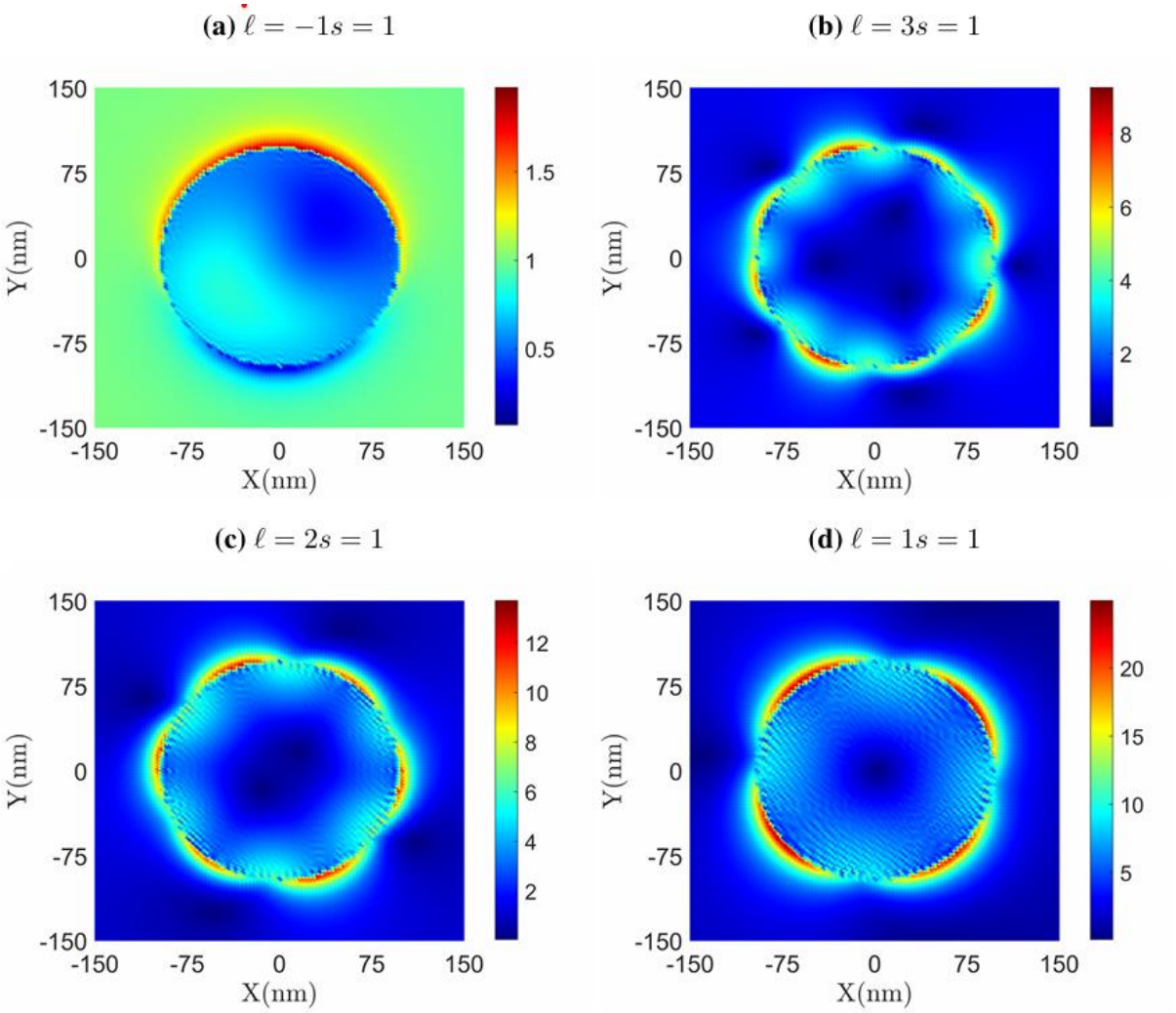


**Figure 3.3 :** The near field distribution of gold nanoplate in four cases.

## b. The dependence of MPR on size parameter

To fully understand the multipole plasmonic effect we compare the absorption and scattering spectrum of gold nanoplates with different radii and thicknesses in Figure 3.4 and Figure 3.5 respectively. $LG_{11}$ mode is used in this simulation. Figure 3.4 shows that the scattering peak and the absorption peak have the trend moving to the higher wavelength when the radius increases. This phenomenon is similar to the SPR effect caused by the linear polarization beam. Moreover, the amplitude of the scattering peak shows an increasing trend with the wavelength, meanwhile, the absorption peak shows the highest peak with a radius of 100 nm. This result concludes that the gold circular nanoplate with a radius of 100 nm can create the strongest plasmon resonance. Figure 3.5 shows a decreasing trend in peak wavelength and peak altitude of absorption and scattering peaks when

the nanoplate's thickness increases. Increasing the structure thickness reduces the penetration depth of the incident light and weakens the amplitude of plasmonic resonance. Overall, the multipole plasmonic effect depends a lot on the size parameter of the structure.

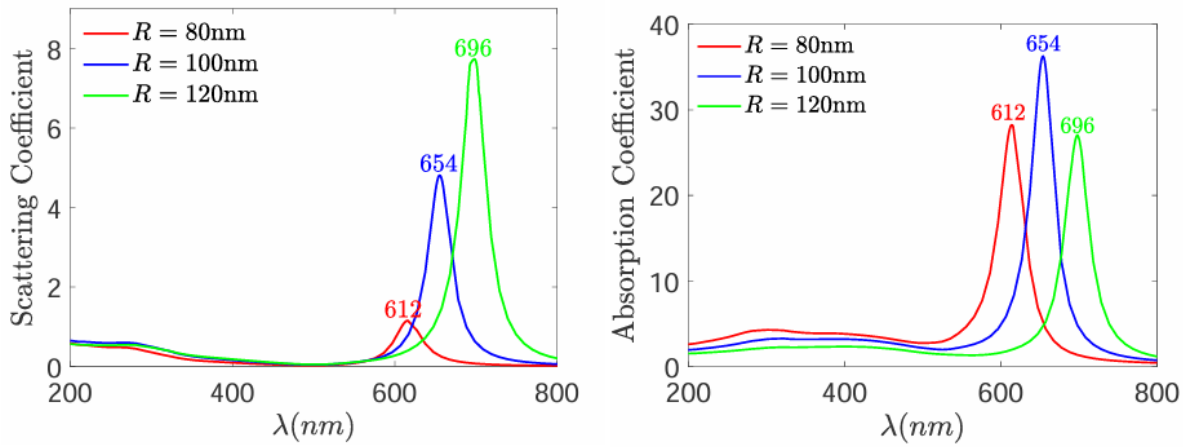


**Figure 3.4:** Absorption and Scattering spectrum of gold nanoplate with R = 80, 100, 120 nm and d = 10 nm.

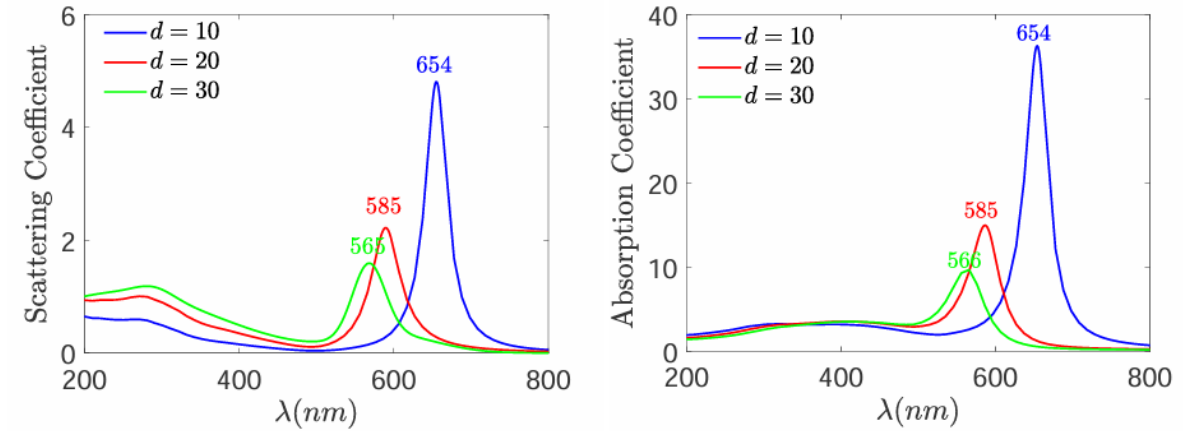


**Figure 3.5:** Absorption and Scattering spectrum of gold nanoplate with d = 10, 20, 30 nm and R = 10 nm

## 3.3 Square gold nanoplate

The circular gold nanoplate has perfectly shown the formation of a multipole plasmonic effect due to its circular symmetry. The absorption, scattering spectrum, and near-field distribution of a gold square nanoplate are observed to investigate the formation of multipole plasmonic resonance in a noncircular symmetry structure. The side length of the square nanoplate in the simulation is 200 nm and the thickness is

10nm.

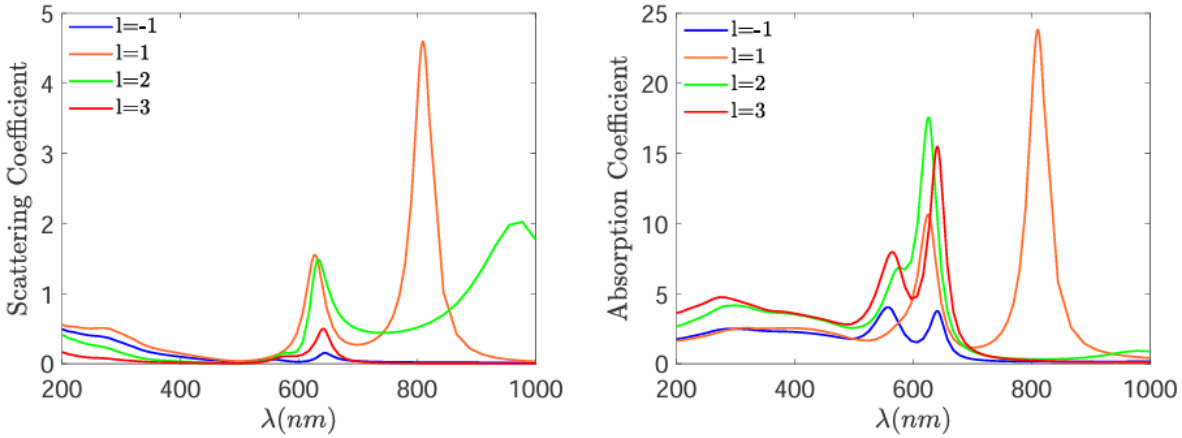


**Figure 3.6:** Absorption and scattering spectrum of gold square nanoplate

Figure 3.6 shows the absorption and scattering spectrum of gold square nanoplate excited with different LG modes. With each mode, they show two absorption peaks. This result was beyond our expectations. The circular plate structure shows only one peak for the multipole plasmon resonance, therefore, we believe that there is a new effect in this structure. However, the spectrums in this case show the same trend as the spectrum in the circular shape when the peak shifts to the lower wavelength when the total angular momentum increases. Figure 3.7 shows the near-field distribution of square gold nanoplate at the absorption peak wavelength to solve this suspect.

Figures 3.7a, 3.7c, and 3.7e show that the multipole plasmonic is created at the lower wavelength in each mode. At the higher wavelengths, the plasmonic effect is localized at the corner of the square plate and the effect of the multipole plasmonic resonance becomes minimal in this situation. These results conclude that the multipole plasmonic effect can be created at a non-circular symmetry structure. However, the localized surface plasmonic resonance can become sig- nificantly greater than the multipole plasmonic effect at the sharp point of the structure and affect most of the structure properties.

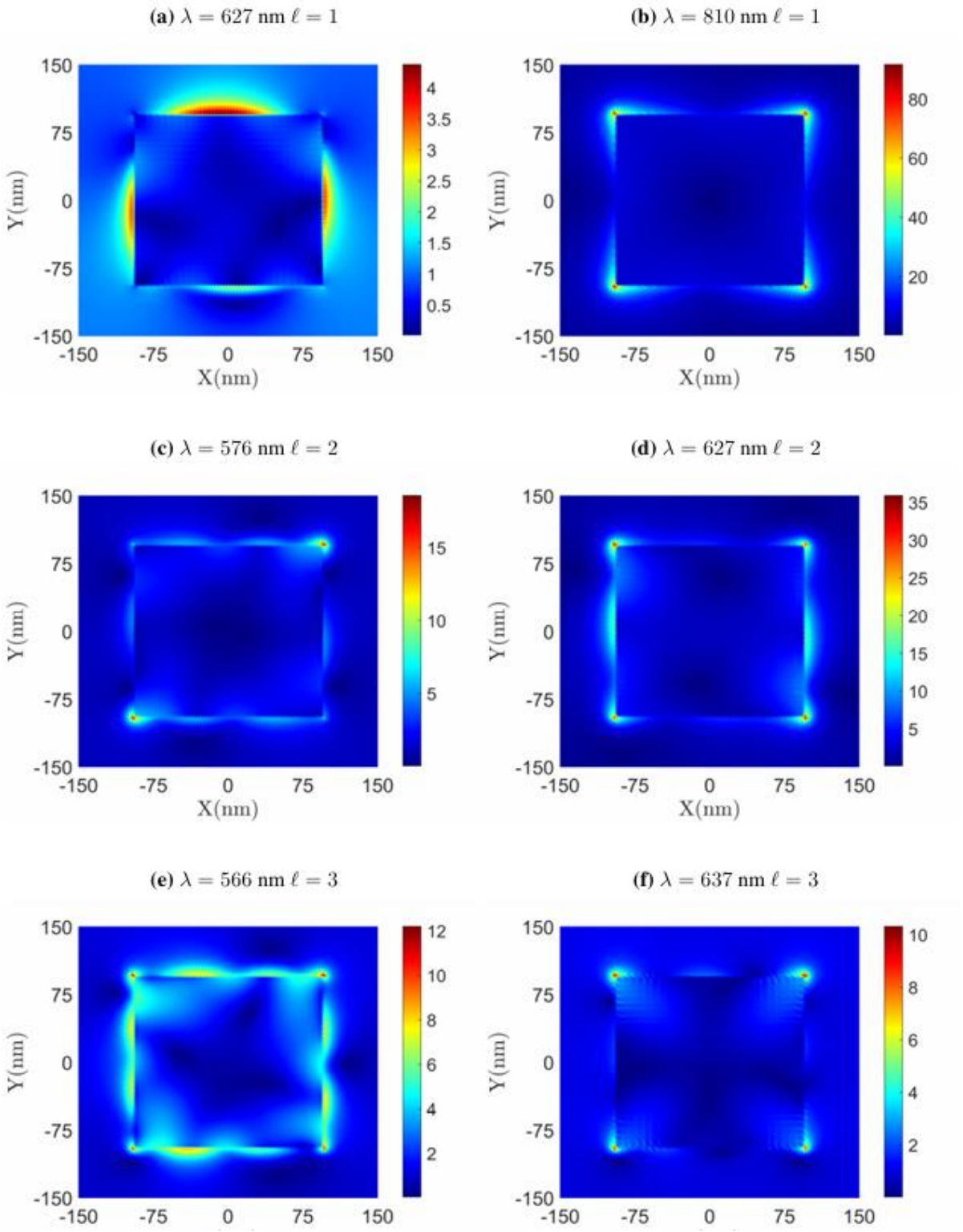


**Figure 3.7:** Near field electric distribution of gold square nanoplate

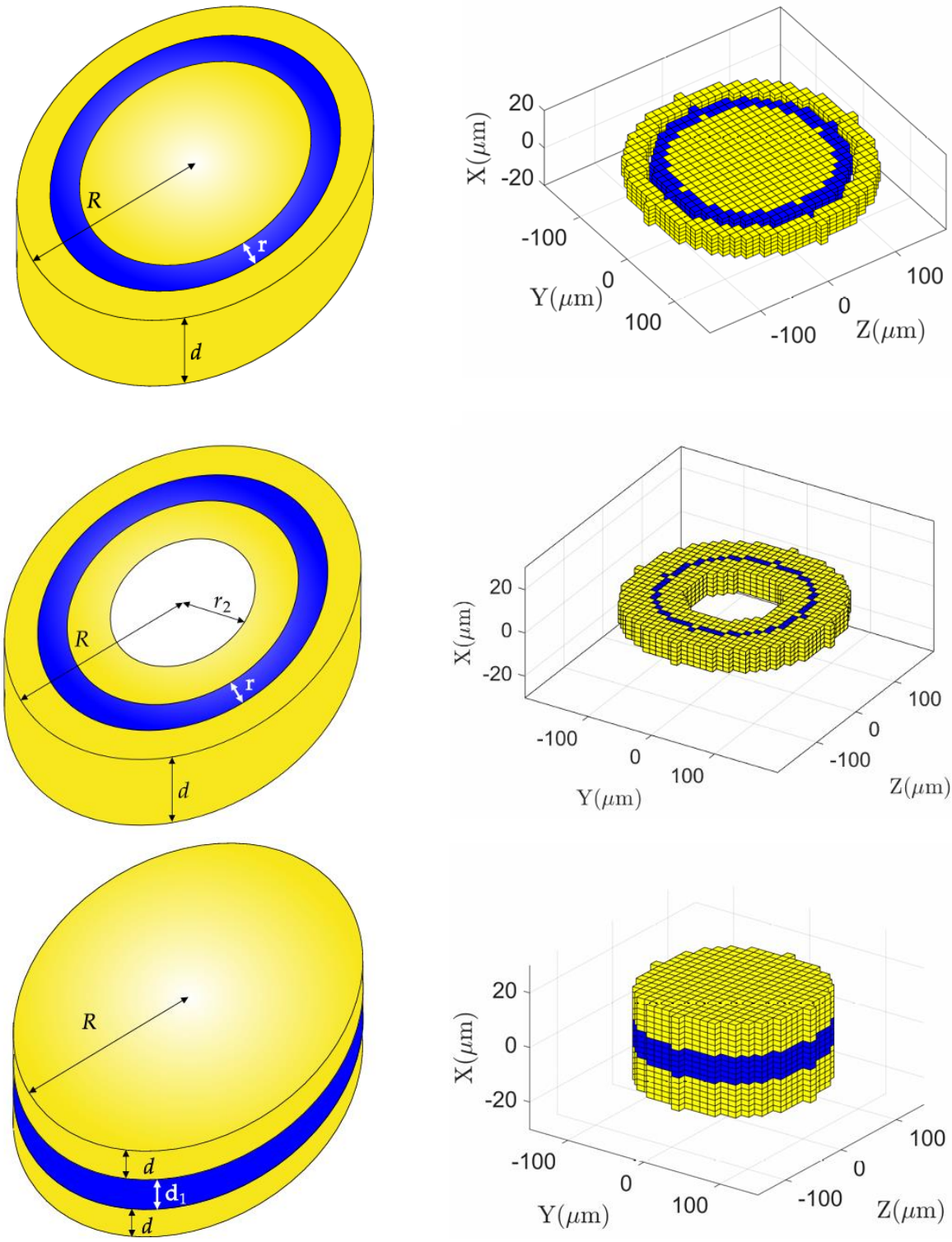


***Figure 3.8:*** *Schematic of MIM model structure. The left picture is the visualization model of the MIM structure. The right picture is the structure after discretized.*

## 3.4 Metal-insulator-metal structure (MIM)

In this part, the interaction of the LG mode with a three-layer structure that consists of gold, insulator, and gold is considered. Three models of Metal-Insulator- Metal

structure (MIM) are investigated in this part. With the first model, the structure consists of a gold nanoplate, a layer of insulator, and a gold ring around the structure. The radius of the total structure is $R = 150$ nm and the radius of the middle layer is $r$ changing from 10 nm to 40 nm. Therefore, the radius of the outer ring changes from 40 nm to 10 nm respectively. The structure thickness is set to $d$=10 nm.

In the second model, we modify the structure of the first model. A hole is created in the middle of the nanoplate and examines the effect of the hole's radius $r_2$ on the absorption and scattering spectrum. The inside hole's radius varies from 30 nm to 70 nm. The thickness of the insulator layer is set to 10 nm to consider the effect of the outer ring. The thickness of all structures is set as 10 nm.

With the last model, we organize the structure with the middle layer as an insulator, the top and bottom layers are gold nanoplate. The radius of the structure is $R = 100$ nm, and the thickness of the gold plate is set as $d = 10$ nm. The middle layer thickness ($d_1$) changes from 4 nm to 16 nm. Figure 3.8 shows all structures' schematic and reduced models after discretized. The $LG_{11}$ mode is used as an excited light source in both cases due to the high absorption and scattering rate shown in the previous part.

### *3.4.1 First structure: Gold plate - Insulator ring - gold ring*

In the first structure, we investigate two cases when the middle layer is vacuum and Poly methyl methacrylate (PMMA). Figures 3.9a and 3.9b show the absorption and scattering spectrum of the first model with vacuum. It shows a decreasing trend in the absorption peak amplitude when decreasing the middle layer radius contrary to the increasing of the scattering peak. However, they both do the red shift when $r$ decreases to 10 nm. These phenomena show that the outer ring does not contribute to the plasmon resonance when $r$ is greater than 10 nm. It fills up the space and limits resonance, which leads to a decrease in the absorption spectrum. However, with $r$ equal to 10 nm, the outside ring interacts with the electric field created by the multipole plasmon resonance and creates a big shift in both the absorption and scattering spectrum. Furthermore, when removing the inner plate, the absorption and scattering spectrum of the outer ring in Figures 3.9c and 3.9d become minimal. This result confirms that the outer ring does not interact directly with the incident light.

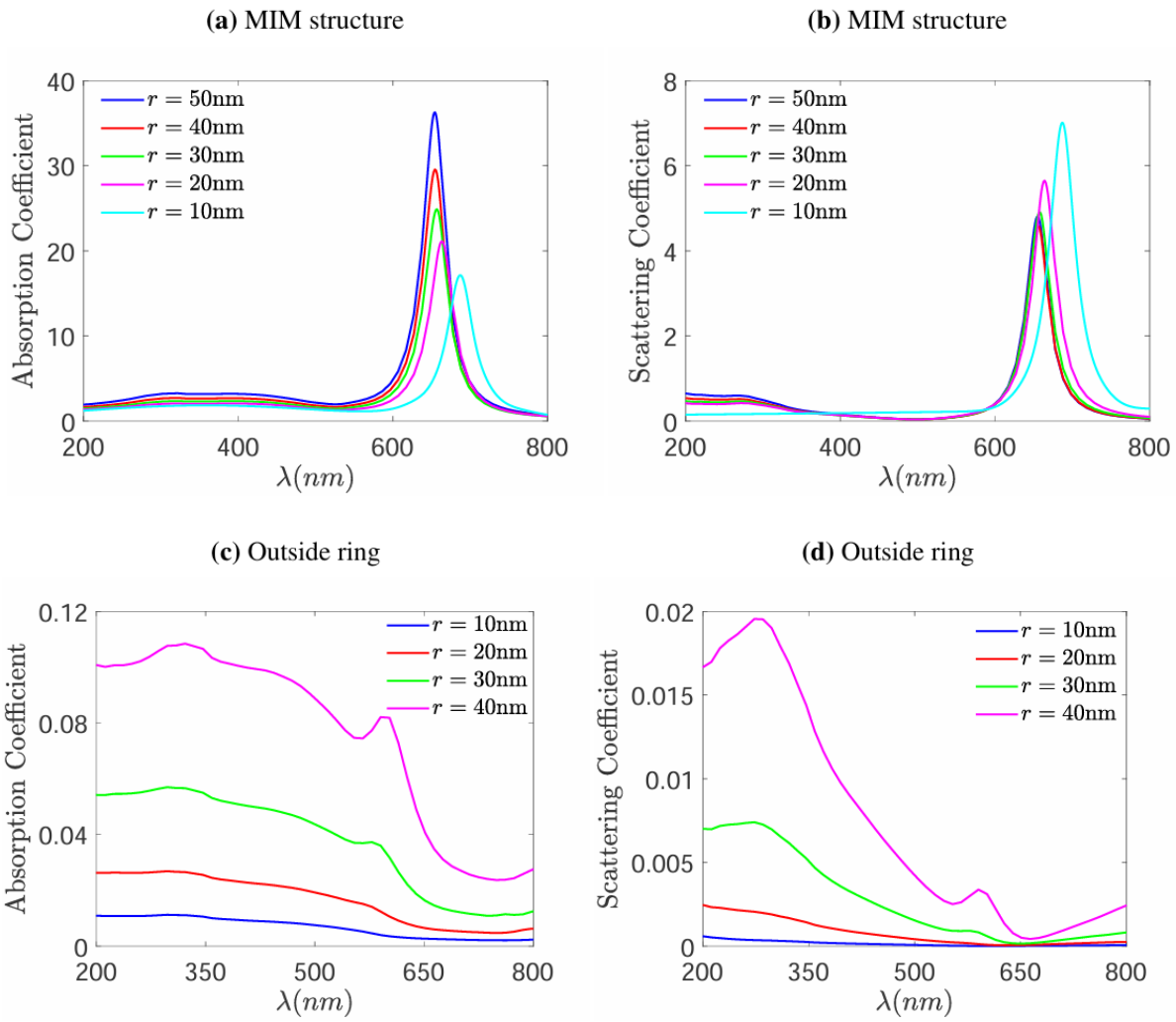


**Figure 3.9:** Absorption and scattering spectrum of MIM (a),(b) and the outside ring only (c)(d). The middle layer in this case is the vacuum.

Figure 3.10 depicts the electric field distribution of the first model. In figure 3.10a the distance between the inner plate and the outside ring is 40 nm, hence, it forms the quadrupole state around the inner plate. This effect is similar to the impact in the single-plate case, therefore, the absorption peak decreases due to the limits of the outside ring. However, in Figure 3.10b the distance between the inner plate and outside ring is reduced to 10 nm. Hence, the nearfield electricity of the inner plate can interact with the outer ring. This interaction creates a quadrupole plasmon resonance at the outside of the structure. This effect explains the shifting peak in Figures 3.9a and 3.9b. Moreover, with this result, we can estimate that the region strongly affected by the nearfield electricity of the inner plate is about 10 nm around the inner plate.

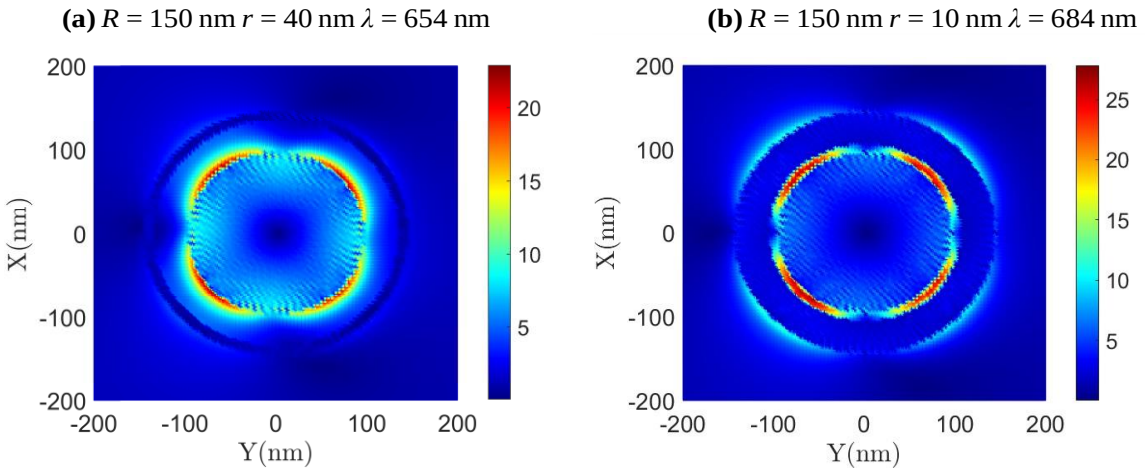


**Figure 3.10:** Electric field distribution of MIM structure at absorption peak.

Figure 3.11 compares the scattering and absorption peak of the first model when filling PMMA to the middle layer and vacuum. Filling up the vacuum layer with PMMA makes the absorption and scattering peak shift to the infrared region. Moreover, the amplitude of the absorption peak increases, meanwhile, the scattering peak decreases. These effects can be explained by the higher refractive index of PMMA material compared to vacuum.

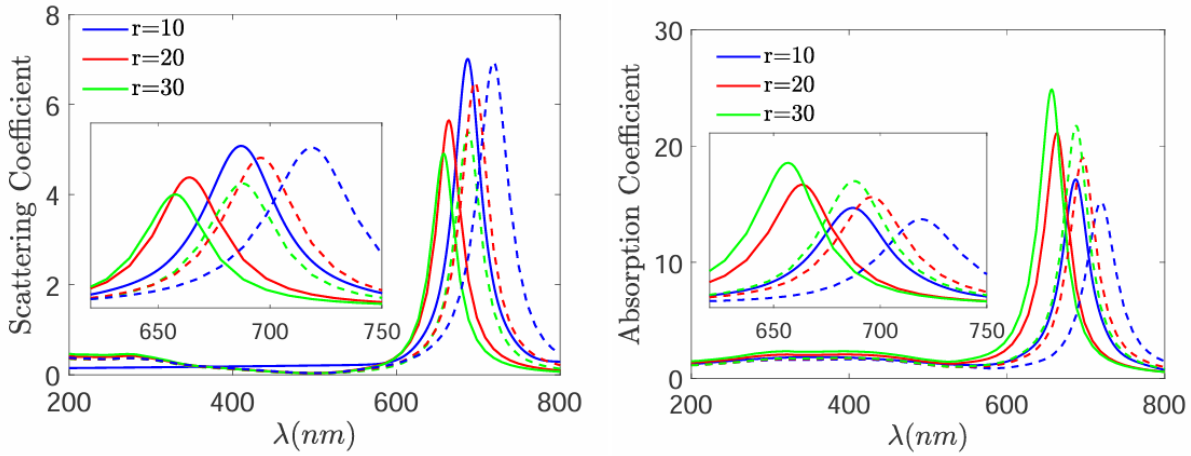


**Figure 3.11:** Absorption and scattering spectrum of the first model with vacuum and PMMA layer at different r. The dashed line shows the result with PMMA and the filled line shows the vacuum result.

### *3.4.2 Second structure: empty gold plate - PMMA ring - gold ring*

In figure 3.12, the red shift is observed in the absorption and scattering spectrum when $r_2$ equals 50 nm and 70 nm. Otherwise, when $r_2$ equals 30 nm the absorption and scattering spectrum change are not trivial. Moreover, the intensity of both spectra shows a decreasing trend when increasing the hole's radius $r_2$. Suppose that the

decreasing trend in the intensity is based on the field distribution of the beam profile. Cause the beam waist is 70 nm and has the singularity point in the optical axis, therefore most of the light intensity focuses on the region from 40 nm to 100 nm. Because of the above setup, most of the light does not interact with the sample when the hole radius is equal to 50 and 70 nm and leads to a decreasing trend in peak amplitude. In addition, we assume that there is a new mode of plasmon resonance inside the hole which causes the huge shift in peak location.

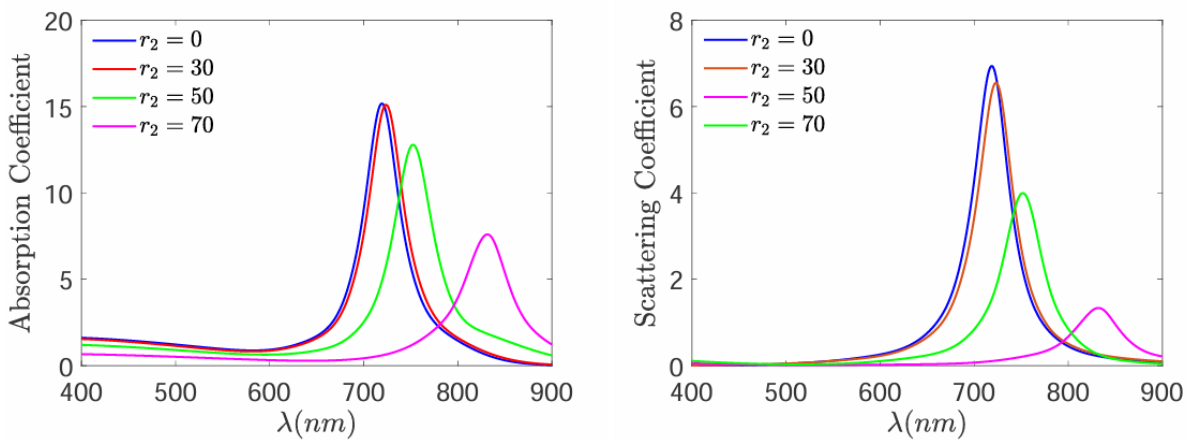


**Figure 3.12:** Absorption and scattering spectrum of the second model depend on the hole's radius.

Figure 3.13 shows the electric distribution when $r_2$ equals 30 nm and 50 nm. Looking at Figure 3.13b the new plasmon resonance mode appears inside the hole of the nanogold plate. However, figure 3.13a does not show any new mode of plasmon resonance. Therefore, we can conclude that the shifting effect is mostly based on the formation of the new plasmon mode.

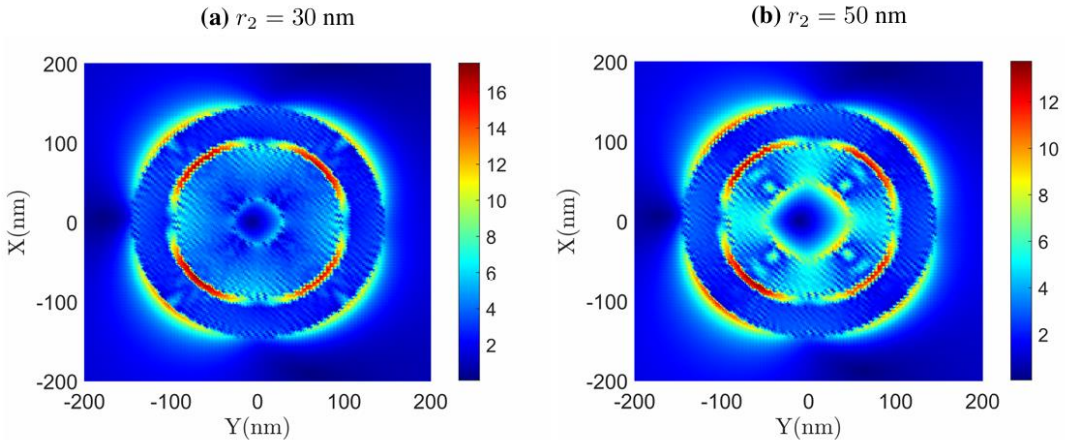


**Figure 3.13:** Electric distribution with different hole radii. The left figure to the right shows electric distribution with $r_2$ equal to 30 nm and 50 nm respectively.

### *3.4.3 Third structure: Sandwich structure*

A single gold nanoplate with $R$ = 100 nm shows the absorption and scattering peak at the wavelength 654 nm, however, with the second structure we observed the peak around 600 nm. The peaks vary from 590 nm to 615 nm when increasing the PMMA layer thickness ($d_1$). This result indicates that there is not only the multipole plasmon effect on the gold nanoplate but also the coupling effect between two gold nanoplates through the PMMA layer.

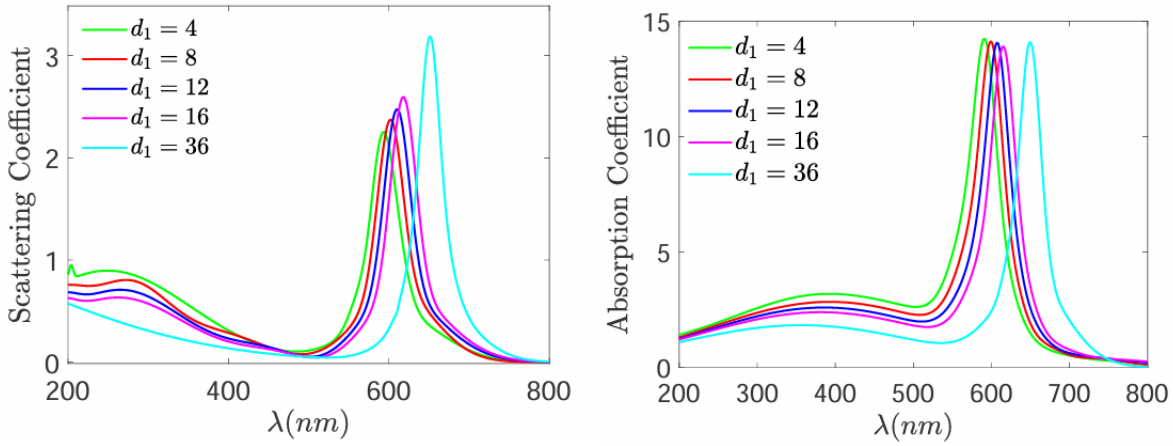


**Figure 3.14:**The sandwich model's Absorption and Scatxtering spectrum depend on the PMMA layer's thickness excited by the LG beam.

In addition, a linear dependence between the resonance wavelength and the thickness of the PMMA layer ($d_1$) is noticed d. In case $d_1$ decreases to 0nm the structure becomes a gold nanoplate with a thickness equal to 20 nm hence we observe the resonance wavelength at 585 nm which had shown in figure 3.5. To confirm our observation, the interaction between structures with $LG_{11}$, $LG_{21}$, $LG_{31}$ and linear polarization light are simulated. The resonance wavelength in each case is reported in the table 3.2.

**Table 3.2.** Table shows the resonance wavelength with different PMMA thicknesses

| $d_1$ | 0 nm | 4 nm | 8 nm | 12 nm | 16 nm | 36 nm |
|---|---|---|---|---|---|---|
| $LG_{11}$ | 585 nm | 593 nm | 602 nm | 609 nm | 618 nm | 651 nm |
| $LG_{21}$ | 545 nm | 550 nm | 558 nm | 566 nm | 573 nm | 601nm |
| $LG_{31}$ | 531 nm | 535 nm | 541 nm | 548 nm | 555 nm | 579 nm |
| Linear | 514 nm | 520 nm | 525 nm | 530 nm | 535 nm | 562 nm |

Figure 3.15 displays the result of Table 3.2 and shows in detail the linear dependence between PMMA thickness ($d_1$) and resonance wavelength ($\lambda$). All modes of the incident light source show a linear relation. Hence, we believe that the main factor leading to this effect is based on the structure of the sample.

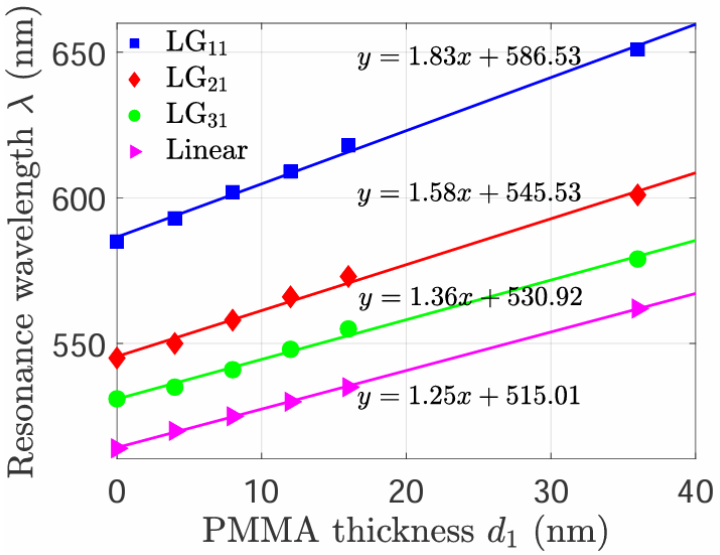


**Figure 3.15:** The linear dependence between resonance wavelength and the PMMA thickness.

For a deeper understanding, we display the electric field distribution cross-section that cuts through the sample in Figure 3.16. Figure 3.16b shows that the PMMA layer acts as the channel to store energy and enhance the coupling effect between two gold layers. Figures 3.16c and 3.16d show the quadrupole state of the plasmon resonance. This result again approves the selective rule shown in the previous part.

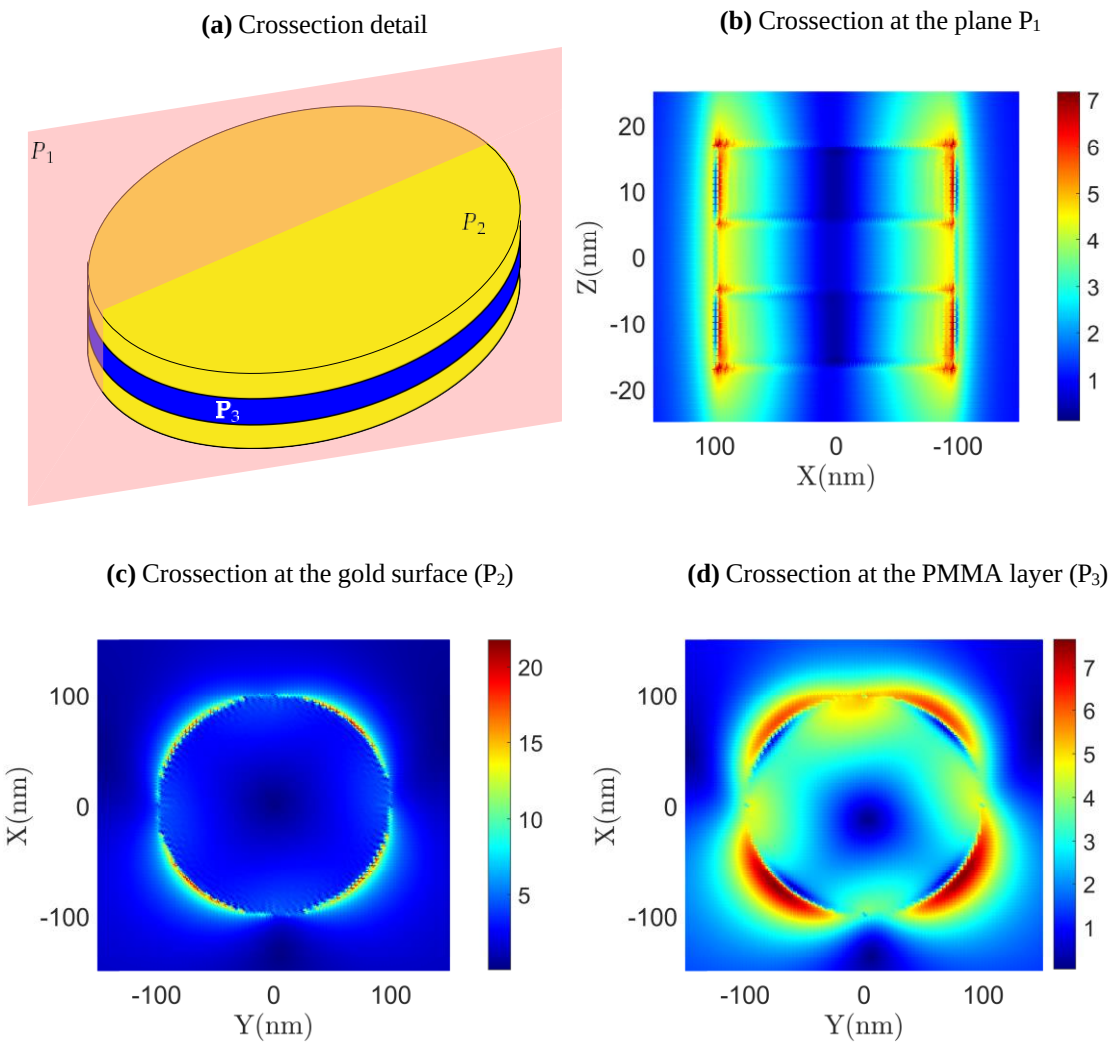


**Figure 3.16:** Crossection electric field distribution. (a) Along the sample. (b) On the gold surface. (c) On the PMMA layer.

# CHAPTER 4: RESULTS AND CONCLUSIONS

The main results of the thesis are:

- Successfully simulated the interaction of OVs (LG mode) with metal (gold) nanostructure using DDSCAT program.
- Showing the dependence of wavelength and the amplitude of the multipole plasmon resonance peak on the shape, size of a single gold nanoplate, and the TAM of the OVs.
- Verified the linking rule between the state of multipole plasmon resonance and the TAM of the LG mode.
- Giving a general description of the interaction between the OVs and MIM when modifying the structure parameter.

These results describe the fundamental interaction of OVs with metal nanostructure and can be used as a base for deeper study in multipole plasmons and optical vortex. In the future, we expect to set up an experiment to confirm the simulation result and give a more detailed description of the MSPR effect.

## APPENDIX A. DDSCAT theory

### Propagation equation of electric field

We usetheHelmholtz equation which is based on the Maxwell equation to simulate the propagation and interaction of the electromagnetic wave with material:

$$\nabla \times \nabla \times \mathbf{E}(\mathbf{r}, \boldsymbol{t}) + \frac{\mu(\mathbf{r})\varepsilon(\mathbf{r})}{c_0^2}\frac{\partial^2 E(r,t)}{\partial t^2} = 0 \tag{A.1}$$

where $k^2(\mathbf{r}) = \omega^2\mu(\mathbf{r})\varepsilon(\mathbf{r})/c^2$. $\mu(\mathbf{r})$ and $\varepsilon(\mathbf{r})$ are the magnetic permeability and electric permittivity respectively. We use the volume integral equation method to solve the above equation. Hence, we define a volume-current density as:

$$\mathbf{J}(\mathbf{r}) = \begin{cases} -\mathrm{i}\omega\varepsilon_0[\varepsilon(\mathbf{r}) - 1]\mathbf{E}(\mathbf{r}) & (\mathbf{r} \in \Gamma_-) \\ 0 & (\mathbf{r} \in \Gamma_+) \end{cases} \tag{A.2}$$

$\Gamma_-$ and $\Gamma_+$ are the space inside and outside the sample respectively. We do not consider the magnetism material or the parameter μ(r) = 1. We can represent the E(r)ε(r) through the current density volume as:

$$\mathbf{E}(\mathbf{r})\varepsilon(\mathbf{r}) = \mathbf{J}(\mathbf{r})\frac{\mathrm{i}}{\omega\varepsilon_0} + \mathbf{E}(\mathbf{r}) \tag{A.3}$$

Substitute equation (A.3) to the equation (A.1) we get:

$$\nabla \times \nabla \times \mathbf{E}(\mathbf{r}) - k_0^2\mathbf{E}(\mathbf{r}) = \mathrm{i}\omega\mu_0\mathbf{J}(\mathbf{r})$$

$$(\nabla \times \nabla \times I - k_0^2)\mathbf{E}(\mathbf{r}) = \mathrm{i}\omega\mu_0\mathbf{J}(\mathbf{r})$$

I is the identity matrix, hence, the operator $(\nabla \times \nabla \times I - k_0^2)$ is a linear operator. We use the Green function $(\mathbf{G}(\mathbf{r}, \mathbf{r'}))$ method to solve the above equation. So, we get two equations:

$$\begin{cases} (\nabla \times \nabla \times I - k_0^2).\mathbf{G}(\mathbf{r}, \mathbf{r'}) = \delta(\mathbf{r} - \mathbf{r'}) \\ \mathbf{E}(\mathbf{r}) = \mathrm{i}\omega\mu_0 \int_{\Gamma_-} \mathbf{G}(\mathbf{r}, \mathbf{r'}).\mathbf{J}(\mathbf{r'})d\mathbf{r}^3 + \mathbf{E}_{inc}(\mathbf{r}) \end{cases} \tag{A.4}$$

The solution of the Green function to equation (A.4) is found analytically as:

$$\mathbf{G_0}(\mathbf{r},\mathbf{r}') = \left[\mathrm{I} + \frac{1}{k_0}\nabla^2\right]\frac{\exp\left(ik_0|\mathbf{r}-\mathbf{r}'|\right)}{4\pi|\mathbf{r}-\mathbf{r}'|}$$

**Approximation of Green function**

We consider an integral $\int_V \mathbf{G}(\mathbf{r_0},\mathbf{r}')\mathbf{J}(\mathbf{r}')$ where $r_0$ is the point in $V$ and $V \subset \Gamma_-$. We can split the above integral into three parts:

$$\int_V \mathbf{G}(\mathbf{r_0},\mathbf{r}')\mathbf{J}(\mathbf{r}')\,\mathrm{d}\mathbf{r}'^3$$

$$= \int_{V/V_0} \mathbf{G}(\mathbf{r_0},\mathbf{r}')\mathbf{J}(\mathbf{r}')\,\mathrm{d}\mathbf{r}'^3 + \int_{V_0} \mathbf{G}(\mathbf{r_0},\mathbf{r}')\mathbf{J}(\mathbf{r}') - \mathbf{G_s}(\mathbf{r}_0,\mathbf{r}')\mathbf{J}(\mathbf{r}')\,\mathrm{d}\mathbf{r}'^3$$

$$+ \frac{1}{k_0^2}\oint_{\partial V_0} -\mathbf{n}\left[\frac{\mathbf{r}-\mathbf{r_0}}{4\pi\,|\mathbf{r}-\mathbf{r_0}|}\mathbf{J}(\mathbf{r_0})\right]$$

The first term is the integral of the volume outside $V_0$ . The second term presents the volume inside $V_0$ but does not contain the surface of $V_0$ and $G_s(\mathbf{r_0},\mathbf{r}') = \frac{1}{k_0^2}\nabla\nabla\frac{1}{4\pi|\mathbf{r}'-\mathbf{r_0}|}$ The last term shows the effect of the surface V0. But when we discrete the volume $\Gamma_-$ to several small cubes $V \approx V_0$ then the first term becomes 0. At this point, we can replace V0 with V. We can consider the electric current J(r) = J(r0) over all the volume V because V is very small compared to the wavelength. Hence, we get:

$$\int_V \mathbf{G}(\mathbf{r_0},\mathbf{r}')(\varepsilon(\mathbf{r}')-1)\mathbf{J}(\mathbf{r}')\,\mathrm{d}\mathbf{r}'^3 = [\mathbf{M} - \frac{1}{k_0^2}\mathbf{L}]\mathbf{J}(\boldsymbol{r}_0)$$

$$\mathbf{M} = \mathbf{J}(\mathbf{r}_0)\int_{V_0} \mathbf{G}(\mathbf{r_0},\mathbf{r}') - \mathbf{G_s}(\mathbf{r}_0,\mathbf{r}')\,\mathrm{d}\mathbf{r}'^3$$

$$\mathbf{L} = \mathbf{J}(\mathbf{r}_0)\oint_{\partial V_0} -\mathbf{n}\left[\frac{\mathbf{r}-\mathbf{r_0}}{4\pi\,|\mathbf{r}-\mathbf{r_0}|}\right]\mathrm{d}\mathbf{r}'^2$$

**Discrete Dipole Approximation (DDA)**

We discretize the volume Γ− into M cubes. Hence, the equation (A.4) become the summation as:

$$\mathbf{E}(\mathbf{r}) = \mathrm{i}\omega\mu_0 \sum_{k=1}^{M} \int_{V_k} \mathbf{G}(\mathbf{r}, \mathbf{r}')\mathbf{J}(\mathbf{r}')\mathrm{d}\mathbf{r}^3 + \mathbf{E}_{inc}(\mathbf{r})$$

We subtract the effect of the volume Vm on both sides and get:

$$\mathbf{E}(\mathbf{r}) - \mathrm{i}\omega\mu_0 \int_{V_m} \mathbf{G}(\mathbf{r}, \mathbf{r}')\mathbf{J}(\mathbf{r}')\mathrm{d}\mathbf{r}^3 = \mathrm{i}\omega\mu_0 \sum_{\substack{k=1 \\ k\neq m}}^{M} \int_{V_k} \mathbf{G}(\mathbf{r}, \mathbf{r}')\mathbf{J}(\mathbf{r}')\mathrm{d}\mathbf{r}^3 + \mathbf{E}_{inc}(\mathbf{r})$$

The right-hand side of the above equation shows the extinction light with the vol ume Vm because it has the incident field and the scattering field of the other cube to the m cube. So we can rewrite it as:

$$E_m^{exc} = E_m^{inc} - \mathrm{i}\omega\mu_0 \left( M_m - \frac{1}{k_0^2}\, \mathbf{L}_m \right) \mathbf{J}_\mathrm{m}$$

Substitue the equation (A.1) into above equation we get:

$$E_m^{exc} = E_m^{inc} - \omega^2\mu_0\varepsilon_0 \left( M_m - \frac{1}{k_0^2}\, Lm \right) (\varepsilon_m - 1) E_m^{exc}$$

This equation forms a system of linear equations and can be solved numerically.

## APPENDIX B.GENERATE CIRCULAR DISK C CODE

```
#include<stdio.h>

#include <math.h>

int num=0, a = 1, b = 2;

float a1x, a1y, a1z, a2x, a2y, a2z, xmax, ymax;

float zmax, dx, dy, dz, xc, yc, zc, dis;

void setup_Tfaxis (){a1x = 1;a1y = 0; a1z = 0;a2x = 0;a2y = 1;a2z = 0;}

void setup_Space (){dx=1;dy=1;dz=1; xmax=30/dx;ymax=150/dy;zmax=150/dz;}

int main(){

setup_TFaxis(); setup_Space(); FILE*out1,*out2;

out1 = fopen("shape.dat","w");

out2 = fopen("shape.txt","w");

for (int i=1; i<=1000000;i++){

for(int idx = -xmax;idx<=xmax;idx++){

for(int idy = -ymax;idy<=ymax;idy++){

for(int idz = -zmax;idz<=zmax;idz++){

xc = idx*dx;yc = idy*dy;zc = idz*dz;dis = yc*yc + zc*zc;

if(dis<=100*100&&xc<=5&&xc>=-5){

fprintf(out2,"%d\t %d\t %d\t %d\t %d\t %d\t

        %d\n",i,idx,idy,idz,a,a,a);

num++;i++;}}}}

break;}}
```

## APPENDIX C.ROUGH ESTIMATION OF SPR

We consider a sphere gold particle with a radius *R*. Because gold is metal, it has a lot of free electrons. Hence, we can consider gold particles as two spheres of positive gold ions and free electrons. We assume that these two spheres have homogenous charge distribution.

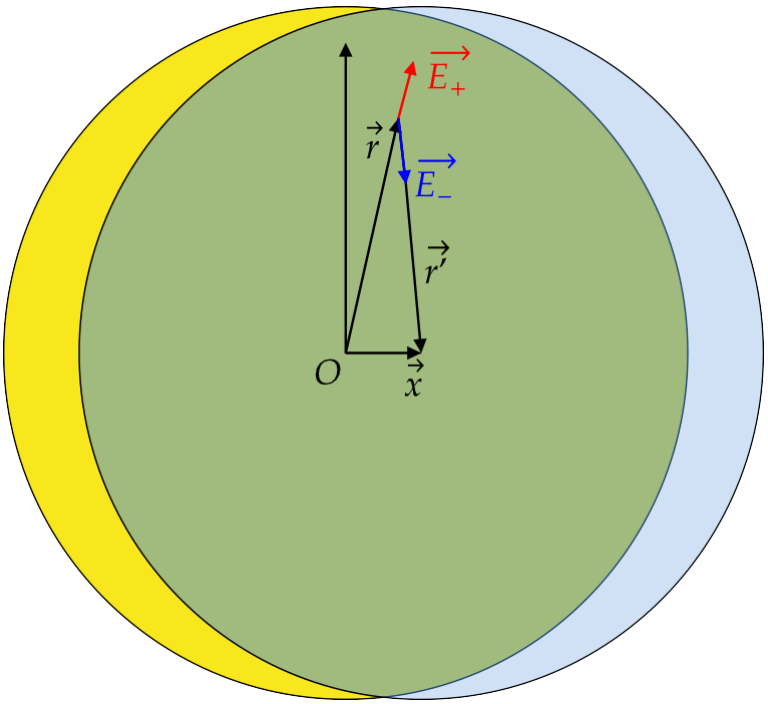


**Figure C.1:** The schematic for normal model of SPR effect.

We consider the position **r** in the neutral part. Using Gauss law we can easily get the electric field at position *r* caused by the ion sphere and the free electron sphere as:

$$\begin{cases} E_{pos} = \dfrac{\frac{4}{3}\pi r^3 ne}{4\pi\varepsilon_0 r^2}\mathbf{e}_r = \dfrac{ne}{3\varepsilon_0}\mathbf{r} \\ E_{neg} = \dfrac{\frac{4}{3}\pi r'^3 ne}{4\pi\varepsilon_0 r'^2}\mathbf{e}_r = \dfrac{ne}{3\varepsilon_0}\mathbf{r}' \end{cases}$$

n in the above equation is electron concentration. Because each gold particle has one free electron per atom, so, we can assume that the electron concentration is equal to the ion concentration. From that result, we can calculate the electric field at point **r** as:

$$\mathbf{E}_{tot} = \mathbf{E}_{pos} + \mathbf{E}_{neg} = \frac{ne}{3\varepsilon_0}\mathbf{x}$$

If we assume that the displacement *x* of the free electron sphere is very small compared with the radius *R* then most of the electron is still inside the ion sphere, hence the Culoumb force put on the free electron sphere can be considered as:

$$\mathrm{F} = -q\mathrm{E}_{tot} = \frac{qne}{3\varepsilon_0}\mathrm{x} = m_e n\ddot{x} \leftrightarrow \ddot{x} = \frac{ne^2}{3\varepsilon_0 m_e}x$$

From this equation, we collect the oscillation frequency $\omega_p = \sqrt{\frac{ne^2}{3\varepsilon\, m_e}}$. Substitutes the gold ion concentration as:

$$n = \frac{d}{M_{Au}}N_A = \frac{19.3}{197} \times 6.022 \times 10^{23} = 5.8997 \times 10^{22}(\text{particles/cm}^3)$$

we get the resonance wavelength at 238nm. This result explains why metal material has a high absorption rate in the ultraviolet region. However, this model doesn't fully describe the Plasmon effect when the surface effect of the material and the ambient medium are not considered. To fully describe the interaction of light with nanoparticles we can use Mie theory for spherical structure and numerical simulation for other shapes.

# APPENDIX D.DISCRETE DIPOLE SCATTERING PROGRAM

## Introduction to DDSCAT

Discrete Dipole Scattering or DDSCAT is an open-source code to calculate the absorption and scattering of light. This code was written by Bruce T. Draine and Piotr J. Flatau in 1998 in the Fortran language. This program calculates the absorption and scattering of light by solving the Maxwell equation using the volume-integral method and discrete dipole approximation. This method does not require discrete the whole space into spices but only discrete the sample volume. So, this program is suitable for optical problems. However, the drawback of this method is the high complexity which approximates $O(x^{3+3\alpha} \log x)$ with $x$ as the number of dipoles and $\alpha$ is smaller than 1. So, this method is suitable for calculating the optical properties of nanoparticles. We can download the source code from "https://ddscat.wikidot.com/".

## Simulation process with DDSCAT

### *Create the structure: "shape.dat"*

The first step to start simulating with the DDSCAT program is to create the nanostructure. We can use the available structure in the code or create the structure by ourselves. The information about the structure is saved in the "shape.dat" file. In this file, we define the number of dipoles to create the structure and distance between two dipoles. the following line consists of 7 numbers. The first number is the index of the dipole, the next three ones represent the positions and the last three numbers express the type of refractive index in three directions for each dipole. We create C code for this purpose. The code to make gold nanodisk is written in the appendix B

***Create source file: "evale.f90"***

With a default DDSCAT program, the incident light is set to be the plane wave with linear polarization. We must edit the source code in the file "evale.f90" to change the source type. The electric field profile in the "evale.f90" file is expressed through the matrix "CXE00(M,ID)". M is the number from 1 to 3 present for the direction and ID is the index number of dipole. After that, we compile the code to create the new "ddscat.exe" executive file to start the simulation.

***Parmeter file: "ddscat.par"***

File "ddscat.par" contains the condition of the simulation such as the range of wavelength, number of materials, index of the ambient environment, etc. For more details, we can find them in the DDSCAT guidelines.

***Result file: "qtable.out"***

The result of DDSCAT is written on the "qtable.out" file. This file contains the extinction, absorption, and scattering cross-section coefficient divided by $\pi a_{eff}^2$ with $a_{\text{eff}}$ as the effective radius of the sample. The near-field information is stored in the "w000r000k000.E1" file. We run the "ddpostprocess.exe" executive file to export the electric distribution result. Each line of the result file consists of ten numbers. The first number is the index number, the next three ones are the position of the point. The six remaining numbers represent the electric field.

# REFERENCES


[1]Review paper is available from J. Opt. Soc. Am. site. Draine, B.T., & Flatau, P.J., "Discrete dipole approximation for scattering calculations", J. Opt. Soc. Am. A, 11, 1491-1499 (1994)

[2]P. J. Flatau and B. T. Draine, "Fast near field calculations in the discrete dipole approximation for regular rectilinear grids," Opt. Express 20, 1247- 1252 (2012)

[3]Kahnert, F. Michael. "Numerical methods in electromagnetic scattering the- ory." Journal of Quantitative Spectroscopy and Radiative Transfer 79 (2003): 775-824.

[4]Yurkin, Maxim A., and Alfons G. Hoekstra. "The discrete dipole approxima- tion: an overview and recent developments." Journal of Quantitative Spec- troscopy and Radiative Transfer 106.1-3 (2007): 558-589.

[5]Louis, Catherine, and O. Pluchery. "Gold nanoparticles in the past: before the nanotechnology era." Gold nanoparticles for physics, chemistry and biology 1 (2012).

[6]Singh, Jagpreet, et al. "Biogenic synthesis of silver nanoparticles and its photocatalytic applications for removal of organic pollutants in water." Journal of Industrial and Engineering Chemistry 80 (2019): 247-257.

[7]Chen, Xi, et al. "Visible-light-driven oxidation of organic contaminants in air with gold nanoparticle catalysts on oxide supports." ANGEWANDTE CHEMIE-INTERNATIONAL EDITION IN ENGLISH- 47.29 (2008): 5353.

[8]Gong, Leibo, et al. "Plasmonic platinum nanoparticles–tungsten oxide nano architectures as visible light photocatalysts for highly efficient overall water splitting." Journal of Materials Chemistry A 10.39 (2022): 21161-21176.

[9]Xie, Liping, et al. "State of the art in flexible SERS sensors toward label-free and onsite detection: from design to applications." Nano Research 15.5 (2022): 4374-4394.

[10]Brongersma, Mark L., and Pieter G. Kik, eds. Surface plasmon nanophotonics. Vol. 131. Springer, 2007.

[11]Weng, Guojun, et al. "Multipole plasmon resonance in gold nanobipyramid: Effects of tip shape and size." Physics Letters A 412 (2021): 127577.

[12]Habteyes, Terefe G., et al. "Theta-shaped plasmonic nanostructures: bringing "dark" multipole plasmon resonances into action via conductive coupling." Nano letters 11.4 (2011): 1819-1825.

[13]Shen, Yijie, et al. "Optical vortices 30 years on: OAM manipulation from topological charge to multiple singularities." Light: Science & Applications 8.1 (2019): 90.

[14]Wang, Jian, et al. "Optical Fiber Telecommunications VIB: Chapter 12. Mul-timode Communications Using Orbital Angular Momentum." (2013).

[15]Padgett, Miles, and Richard Bowman. "Tweezers with a twist." Nature pho- tonics

5.6 (2011): 343-348.
[16]Dienerowitz, Maria, et al. “Optical vortex trap for resonant confinement of metal nanoparticles.” Optics express 16.7 (2008): 4991-4999.
[17]Ren, Yongxiong, et al. “Orbital angular momentum-based space division multiplexing for high-capacity underwater optical communications.” Scientific reports 6.1 (2016): 33306.
[18]Wang, Jian. “Advances in communications using optical vortices.” Photonics Research 4.5 (2016): B14-B28.
[19]Johnson, Peter B., and R-WJPrB Christy. “Optical constants of the noble metals.” Physical review B 6.12 (1972): 4370.
[20]Sakai, Kyosuke, et al. “Excitation of multipole plasmons by optical vortex beams.” Scientific reports 5.1 (2015): 8431.
[21]Rosen, Joseph, ed. “Holography:Recent Advances and Applications.” (2023).
[22]Wilcox, Christopher C., et al. “Adaptive optical system atmospheric turbulence generator testbed.” Proc. 2007 AMOS Technical Conf. 2007.